跨領域神經科學國際研究生博士學位學程

國立臺灣大學生命科學院

博士論文

Taiwan International Graduate Program in Interdisciplinary Neuroscience

College of Life Science

National Taiwan University

Doctoral Dissertation

研究 *C9ORF72* 漸凍人症中富含精胺酸雙胜肽所造成的細胞核 TDP-43 蛋白凝集現象

The study of TDP-43 nuclear condensation under *C9ORF72* ALS-associated arginine-rich dipeptides

迪 莎

Diksha Agnihotri

指導教授：黃人則博士

共同指導教授：黃憲松博士

Advisor: Joseph Jen-Tse Huang, PhD.

Co-advisor: Hsien-Sung Huang, Ph.D.

中華民國 113 年 10 月

October 2024

doi:10.6342/NTU202500138

Acknowledgement

I would like to express my deepest gratitude to my advisor Dr. Joseph Jen-Tse Huang and my co-advisor Dr. Hsien-Sung Huang whose valuable suggestions and expertise helped me to enhance my scientific knowledge eventually leading for the successful completion of my project. I would like to specially thank Dr. Joseph Jen-Tse Huang for being my true mentor and listening to my ideas as a friend. He always motivated me to be fearless and confident throughout my PhD journey. I would also like to thank my committee members Dr. Yijuang Chern, Dr. Hung-Chih Kuo, Dr. Jun-An Chen, Dr. Woan-Yuh Tarn for their valuable suggestions and sincerely pointing out the insufficiencies in my work for further improvements.

I would also like to sincerely thank the people from my lab for helping me finalize the project. The expert advice and constructive suggestions from the post-doctoral of my lab, Dr. Chi-Chang Lee, Dr. Ruei-Yu He, Dr. Yung-An Huang, Dr. Bryan always helped me in improving my project and knowledge. They always supported me during the hard times and when I was facing difficulty. I would also like to thank the other PhD students of my lab Po-Chao Lu, Dr. Hung-Ming Chien, Steven for discussing about my project and giving ideas for further improvements. In addition, I want to thank Brandon and Eric for helping me to seed the cells for my experiments especially during the revision of our manuscript. Finally, I would like to thank all my lab mates for being supportive and creating a friendly, warm environment where I enjoyed working the most.

Last but not the least, I would like to thank my parents for providing me emotional support throughout the PhD journey and being my backbone. I would also like to thank my brother

doi:10.6342/NTU202500138

and sister-in-law for listening to my worries at crucial times of the journey. I would also like to thank my friends for being there for me in all the hard times and supporting to keep going. Most importantly, I would like to send my greatest prayers to thank my almighty for the strength he gave me throughout the thick and thins. It is my god who guided my actions to achieve a doctorate title which was once a dream.

doi:10.6342/NTU202500138

Abstract

Amyotrophic Lateral Sclerosis (ALS) is a fatal neurodegenerative disease characterized by motor neuron degeneration that leads to paralysis, typically resulting in a life expectancy of 3-5 years after onset. A significant genetic factor in ALS is the hexanucleotide repeat expansion (GGGGCC) in the *C9ORF72* gene, which results in the translation of five dipeptide repeats (DPRs). Among these, arginine-rich dipeptides toxicity is highly associated with their ability to disrupt liquid-like properties of membraneless organelles (such as the nucleolus and paraspeckles). Liquid-liquid phase separation (LLPS) of low-complexity domain (LCD)-rich proteins is crucial for the formation of these organelles. Dysregulated LLPS in ALS-related proteins like TAR DNA-binding protein 43 (TDP-43) has been linked to ALS pathogenesis, with alterations in LLPS potentially leading to TDP-43 gelation and aggregation under stress. However, the impact of arginine-rich dipeptides on TDP-43 LLPS in the nucleus is still unclear.

In this study, we investigated the transient and prolonged effects of poly-PR and poly-GR dipeptide on TDP-43 nuclear condensation. Our findings indicate that only transient poly-PR stress induces the formation of TDP-43 nuclear condensates (NCs) with decreased fluidity. Of note, the long non-coding RNA *NEAT1* and the HSP70 chaperones demonstrated significant colocalization with TDP-43 NCs under transient poly-PR stress. Through siRNA-mediated depletion, *NEAT1* was found necessary for TDP-43 NCs formation. In addition, pharmacological inhibition of HSP70 suggested its role in maintaining condensate fluidity. Following prolonged exposure to poly-PR stress, *NEAT1* continued to function as a scaffold

doi:10.6342/NTU202500138

for TDP-43 NC formation. However, HSP70 delocalized from these condensates, resulting in further reduced fluidity and subsequent gelation.

By combining fluorescence lifetime-based imaging microscopy and immunofluorescence staining, the presence of TDP-43 oligomers were detected within gel-like NCs. In addition, prolonged poly-PR stress induced TDP-43 proteinopathy including TDP-43 phosphorylation, mislocalization and C-terminal TDP-43 fragments, along with the increased cytotoxicity. This study elucidates a potential toxicity mechanism of poly-PR dipeptide via perturbation of TDP-43 nuclear LLPS along with canonical TDP-43 proteinopathy, and shedding light on the roles of *NEAT1* and HSP70 in the process.

doi:10.6342/NTU202500138

中文摘要

肌萎縮性脊髓側索硬化症（ALS）是一種致命的神經退化性疾病，運動神經元的退化最終會導致癱瘓，患者自疾病發作後的壽命僅剩 3 到 5 年。ALS 的一個重要遺傳原因是 *C9ORF72* 基因中的六核苷酸重複擴增。*C9ORF72* 基因中的 GGGGCC 序列擴增會轉譯為五種重複雙肽（DPR），包括甘胺酸－丙胺酸（poly-GA）、脯胺酸－精胺酸（poly-PR）、甘胺酸－精胺酸（poly-GR）。在這五種 DPR 中，富含精胺酸的雙肽被認為是最具毒性的。特別是 poly-PR 二肽的毒性與其擾亂無膜胞器液體狀性質的能力高度相關。富含低複雜度區域（LCD）的蛋白質進行的液－液相分離（LLPS）是形成與維持無膜胞器（如核仁與側核斑）的基本機制。與 ALS 相關的蛋白質（如 TDP-43）中的 LLPS 失調被認為與 ALS 的致病機制有關。具體來說，LLPS 的改變可能會導致 TDP-43 在細胞質中凝膠化，並在延長壓力下聚集。然而，poly-PR 壓力對 TDP-43 在細胞核中 LLPS 的影響仍不清楚。

本研究中，我們探討了 poly-PR 壓力對 TDP-43 核凝聚的短期與長期影響。我們的研究結果顯示，暫時 poly-PR 壓力會誘導形成流動性降低的 TDP-43 核凝聚體 (NCs)。值得注意的是，長鏈非編碼 RNA *NEAT1* 與 HSP70 分子伴護蛋白在短期 poly-PR 壓力下與 TDP-43 核凝聚體顯著共位。藉由 siRNA 造成減少，發現 *NEAT1* 其對於 TDP-43 核凝聚體（NC）形成是必要的。此外，以藥物抑制 HSP70 顯示其維持凝聚體流動性中的作用。在長期 poly-PR 壓力下，*NEAT1* 繼續作為 TDP-43 核凝聚體形成的支架；然而，HSP70 從這些凝聚體中脫離，導致流動性進一步降低並最終凝膠化。

doi:10.6342/NTU202500138

利用基於螢光壽命的成像顯微鏡結合免疫螢光染色，發現在凝膠狀核凝聚物（NCs）中存在 TDP-43 寡聚物。此外，長期暴露於 poly-PR 壓力下導致了 TDP-43 蛋白病變，其特徵包括 TDP-43 磷酸化、錯位以及 C 末端 TDP-43 片段的出現，並伴隨著細胞毒性的增加。這項研究闡明了 poly-PR 通過干擾 TDP-43 核內 LLPS 以及典型 TDP−43 蛋白病變可能導致的毒性機制，並揭示了 *NEAT1* 和 HSP70 在這一過程中的作用。

doi:10.6342/NTU202500138

Table of Content

doi:10.6342/NTU202500138

doi:10.6342/NTU202500138

doi:10.6342/NTU202500138

doi:10.6342/NTU202500138

List of Figures

doi:10.6342/NTU202500138

doi:10.6342/NTU202500138

List of Supplementary Figures

doi:10.6342/NTU202500138

List of Tables

doi:10.6342/NTU202500138

1. Introduction

1.1 Amyotrophic Lateral Sclerosis

Amyotrophic lateral sclerosis (ALS) also termed as Lou Gehrig's disease is a progressive neurodegenerative disorder characterized by the degeneration of motor neurons.[1] Loss of the upper and lower motor neurons in the motor cortex, in the nuclei of brain stem and the spinal cord anterior horn leads to muscle stiffness, progressive muscular atrophy, and eventual death of the patient due to breathing difficulty.[2] The onset of the disease is between 55 to 75 years of age and patients succumbs to death within 3 to 5 years of diagnosis.[3] The prevalence of ALS cases ranges between 4.1 to 8.4 per 1,00,000 persons globally.[4] Drugs like benzothiazole, riluzole, edaravone, creatine helps to delay the progression rate but no effective treatment for the disease is available yet.[5] Based on the cause, ALS can be classified as either sporadic or familial. While 90% of the total ALS cases are sporadic and occurs due to unknown reasons, familial ALS occurs due to genetic mutations and constitutes 10% of the total ALS cases[6] (Figure 1A). In familial ALS, mutations in genes like Superoxide dismutase 1 (SOD1),[7] Fused in Sarcoma (FUS),[8] TAR-DNA binding protein (TDP-43),[9] *C9ORF72* genes[10] are the causes of the disease. 40% of the ALS patients bear *C9ORF72* mutation, followed by 12% with SOD1 and 4% with either TDP-43 or FUS mutation[11] (Figure 1B).

doi:10.6342/NTU202500138

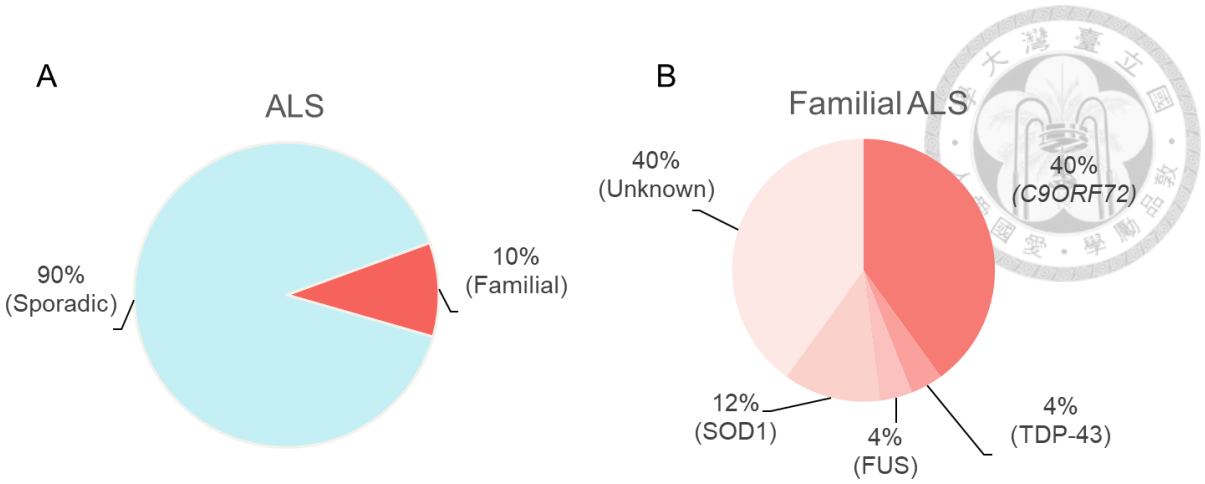

Figure 1. Classification of Amyotrophic lateral sclerosis. (A) Classification of ALS. (B) Familial ALS is further categorized based on the genetic mutations in different genes. Adapted from Yun et al., 2020, Int J Mol Sci.

SOD1 is a copper/zinc metalloenzyme that converts toxic superoxide anion into hydrogen peroxide and molecular oxygen.[12] Mutation in SOD1 gene is correlated with toxic free radical generation in ALS patients.[7] FUS mutation lead to intranuclear toxic aggregate formation of FUS protein which causes neuronal damage.[13] These aggregates disrupt normal RNA-binding functions and interfere with cellular homeostasis, contributing to neurodegeneration. Additionally, they impair stress granule dynamics, further exacerbating cellular dysfunction and neuronal loss in ALS and other related diseases.[14] Mutations in the TDP-43 gene lead to its mislocalization and cytoplasmic aggregation, resulting in a gain-of-function that contributes to neurotoxicity.[9] TDP-43 inclusions are a hallmark of ALS, observed in 97% of patients, encompassing both sporadic and familial cases. The pathological features of TDP-43 include ubiquitination, hyperphosphorylation, and a truncated C-terminus.[15] Mutation in *C9ORF72* gene is the major genetic mutation found in both sporadic (7.7%) and familial (40%) ALS cases and different toxicity mechanisms have been proposed for *C9ORF72*-mediated toxicity.

doi:10.6342/NTU202500138

1.1.1 *C9ORF72* genetic mutation and their associated toxicity in ALS

Chromosome 9 open reading frame 72 (*C9ORF72*) gene contains 11 exons and interspersed intronic regions that encodes for C9ORF72 protein.[16] This protein is involved in several physiological functions. Due to the structural similarity with DENN (differentially expressed in normal and neoplastic cells) proteins, *C9ORF72* act as RabGEF (Guanine Exchange Factor of Rab proteins) controlling membrane trafficking.[17,18] In the *C9ORF72* knockout mice, vulnerability to develop autoimmune disease depicts its important role in maintaining immunity.[19-21] However, in *C9*-ALS and/FTLD, hexanucleotide repeat expansion (HRE) of GGGGCC (G_4C_2) in the first intronic region of the 9p21 FTD/ALS chromosome perturbs the level of *C9ORF72* protein[22,10] (Figure 2). In healthy individuals, the size of G_4C_2 repeat expansion is in the range of 2-10 repeats. While in the *C9ORF72* ALS patients, the range increases to around hundreds of repeats.[16] Due to the expansion in gene, three major toxicity mechanisms are proposed to explain *C9ORF72* genetic mutation. The loss-of-function of *C9ORF72* protein, gain-of-function of *C9ORF72* gene encoded RNA transcripts and gain-of-function of *C9ORF72* gene encoded dipeptide repeat (DPRs) (Figure 2).

doi:10.6342/NTU202500138

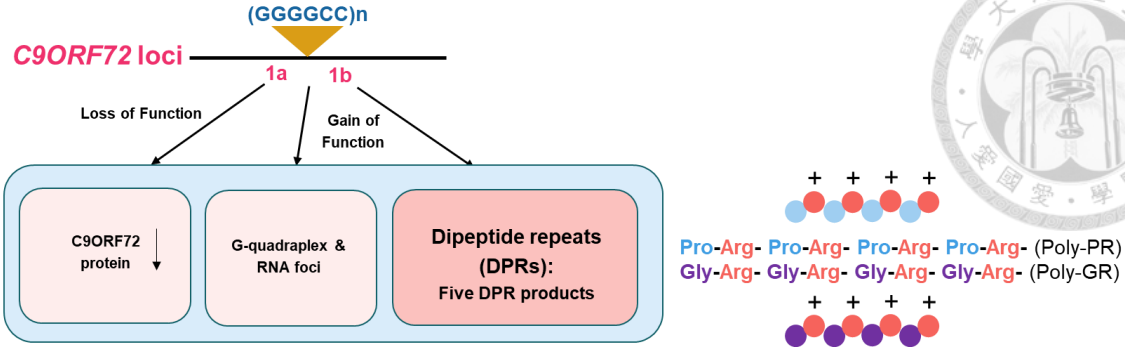

Figure 2. Major toxicity mechanisms of G_4C_2 hexanucleotide expansion in *C9ORF72* gene. Adapted from Tang *et al.*, 2020, Mol. Neurodegener.

1.1.2 Toxic loss-of-function mechanism in *C9ORF72* ALS

C9ORF72 transcript and protein levels are reduced in patients with *C9*-ALS/FTLD.[23-25] Studies indicate that the frontal cortex of ALS and FTLD patients with hexanucleotide repeat expansion shows decreased transcription of *C9ORF72*.[24] For instance, Frick *et al.* reported an 80% reduction in C9ORF72 protein levels in the cerebellum of ALS samples.[26] Additionally, hypermethylation of the G_4C_2 expansion in the *C9ORF72* gene also contributes to its decreased transcription and loss of function.[27] Due to these *C9ORF72* haploinsufficiency, motor deficit in *C9ORF72* ALS/FTD mouse models[28] and axonal degeneration of motor neurons in zebrafish has been observed.[29] Disruption of autophagy pathway through co-aggregation of SQSTM1/p62 with TDP-43 protein inclusions has also been implicated with *C9ORF72* haploinsuffieciency.[30,31] Nonetheless, loss-of-function of *C9ORF72* gene is generally considered to play a lesser role in motor neuron degeneration in ALS patients, with gain-of-function mutations more likely contributing to the disease pathogenesis.

doi:10.6342/NTU202500138

1.1.3 Toxic gain-of-function mechanism in *C9ORF72* ALS

The two important hypotheses for the toxic gain-of-function of *C9ORF72* gene are HRE transcribed RNA foci and translated dipeptide repeats.[32] RNA generated by the repeat expansion accumulate in the nucleus to form aggregated sense and antisense RNA foci in the brain of *C9ORF72* patients. This results in sequestration of proteins like ADARB2, ALYREF, hnRNPH, hnRNPA1, nucleolin, Pur α, and SRSF2 resulting in impaired RNA processing, neuronal mRNA transport impairment.[16] Sequestration of RNA-binding protein in *C9ORF72* generated RNA foci further disrupts nucleocytoplasmic transport, RNA transcription and translation.[16] G-quadraplex structure of *C9ORF72* HRE DNA or RNA lead to generation of truncated RNA transcripts and form RNA hairpin structures.[33] Such structures perturb replication, transcription and translation interfering with RNA processing and causing nucleolar stress.[33-35] In addition to RNA toxicity, translation of toxic DPRs play major role in gain-of-function toxicity mechanism of *C9ORF72* gene.

1.1.4 Dipeptide Repeats (DPRs) toxicity mechanism in ALS

Hexanucleotide repeat expansion in *C9ORF72* gene gives rise to sense and anti-sense RNA. The repeat associated non-ATG (RAN) translation of these RNA encodes for five kinds of peptides namely Poly-GA, Poly-GR, Poly-PR, Poly-GP and Poly-PA.[36,37] Out of the five dipeptides, Poly-GA is moderately toxic and its toxicity is imparted due to its ability to form aggregates leading to sequestration and impairment of nucleocytoplasmic proteins. Colocalization of aggregated poly-GA with HR23A and HR23B nucleocytoplasmic transport

doi:10.6342/NTU202500138

proteins has been observed in mice model which resulted in HR23A and HR23B dysfunction and hence poly-GA mediated neuronal toxicity.[38]

The most toxic dipeptides encoded by the *C9ORF72* gene, arginine-rich Poly-GR and Poly-PR, exert their toxicity by disrupting multiple cellular pathways. Previous studies have reported that both poly-PR and poly-GR dipeptides can form aggregates, though with a lower tendency than poly-GA, resulting in toxic dipeptide inclusions.[37,39,40] Additionally, transfection with PR_{50} has been shown to disrupt nucleolar function by binding to nucleolin, leading to nucleolus perturbation.[41,42] One of the most intriguing toxicity mechanism of arginine-rich dipeptides is their ability to interact with proteins rich in low complexity domain rich (LCDs). This interaction disrupts the dynamic behaviors of membraneless organelles (MLOs) such as nucleoli, stress granules, and P-bodies.[43,44] The formation of MLOs, often described as condensates, occurs through a process called Liquid-liquid phase separation (LLPS).[45,46] LLPS is a biophysical process that enables cellular components to segregate without a membrane, producing specialized environments for various biochemical reactions and stress responses.[45] The perturbation of LLPS has been linked to neurodegenerative conditions, as disrupted LLPS can lead to aberrant condensate formation, mislocalization of essential proteins, and cellular stress.[47,48]

1.1.5 Liquid-Liquid phase separation (LLPS)

Liquid-liquid phase separation (LLPS) is increasingly recognized as the primary mechanism driving the formation of membraneless organelles within cells.[45,49,50] The general mechanism for the formation of these organelles is by the phase separation of the low-complexity domain (LCD) rich proteins from their nuclear or cytoplasmic surrounding.[51]

doi:10.6342/NTU202500138

LCD-rich proteins are enriched in specific amino acids such as glycine, serine, proline, and tyrosine conferring unique physicochemical properties that enables weak multivalent interactions, which promote reversible assembly into dynamic, liquid-like droplets.[52-55] LCD-containing proteins, such as FUS, hnRNPA1, and TDP-43, utilize their intrinsically disordered regions (IDRs) to promote LLPS through a combination of π-π stacking, hydrogen bonding, and cation-π interactions.[45,48] Many of these proteins are RNA-binding proteins (RBPs) and the disordered domains of such proteins promote LLPS in the presence of RNA, enabling the assembly of RNA-protein complexes crucial for RNA metabolism and regulation.[56] LLPS of LCD-rich protein forms membraneless organelles like P bodies, stress granules, Cajal bodies, Paraspeckles, nucleoli.[57] The major function of these organelles is to sequester RNA and/proteins and inhibit their transcription and translation under stress. For example, different kinds of stress like heat, oxidative, endoplasmic reticulum stress, cytoplasmic accumulation of untranslated, 80S ribosome-free mRNAs leads to the formation of RNA foci known as stress granule.[51] Similarly, paraspeckle are another membraneless organelles formed upon stress in nucleus and is built on Nuclear Enriched Abundant Transcript 1 (*NEAT1*) long non-coding RNA.[58] Paraspeckle are also involved in response to various physiological processes like stress response, cell differentiation, cancer progression and differentiation of corpus luteum.[59] In nucleoli, phase separation of nucleolar proteins and RNA molecules helps in organizing the synthesis and processing of ribosomal RNA.[60,61] However, various studies have shown that dysregulation of LLPS upon prolonged stress causes conversion of these liquid-like droplets into gel and finally to aggregate/fiber,[43,62] which is the major cause of ALS. Therefore, understanding the principles of LLPS and the

doi:10.6342/NTU202500138

mechanisms behind aberrant phase separation of proteins is crucial for gaining deeper insights into the disease.

1.1.6 Disruption of LLPS by arginine-rich dipeptides

Arginine-rich dipeptides are most toxic among the five dipeptides encoded by *C9ORF72* gene. Among the various proposed pathways, disruption of LLPS by arginine-rich dipeptides is the crucial toxicity mechanism of poly-PR and poly-GR DPRs (Figure 3).[63] In 2016, Lee *et al.* identified the interactome of poly-PR and poly-GR dipeptide and showed that these dipeptides preferentially interact with LCD proteins, resulting in altered phase separation or aberrant phase transition of these organelles.[42] The phase separated phenylalanine-glycine rich domains of nucleoporins, proteins of nuclear pore complex, undergo aberrant phase transition upon their interaction with poly-PR dipeptide.[44] The binding of Poly-PR dipeptide with phenylalanine glycine rich protein of nuclear pore complex (NPC) results in NPC "clogging" and disruption of nuclear transport.[44] Both arginine-rich dipeptides reduce the liquid-like property of G3BP1, a stress granule protein, contributing to repression of translation.[42,64] Such an alteration in dynamics of stress granule has been correlated with several neurodegenerative disease.[43,65] The fluidity of G3BP1 is reduced upon expression of poly-PR and poly-GR dipeptides.[42] Moreover, arginine-rich DPRs induce stress granule formation and decrease stress granule dynamics leading to disruption of LLPS,[61] indicating major role of these DPRs in *C9ORF72* pathogenesis.

In addition to cytosol, the predominant localization of poly-PR and poly-GR within the nucleus and their interaction with nucleolar protein like NPM1 results in the disruption nucleolar phase dynamics.[42,66,67] Of note, strong binding of poly-PR with acidic tract of

doi:10.6342/NTU202500138

NPM1 disrupt its phase separation, hence nucleolar LLPS (Figure 3).[66] Arginine-rich dipeptides also interact with SRSF7, a protein involved in Cajal bodies formation, reducing the fluidity and disrupting the dynamics of these proteins in nucleus (Figure 3).[42] Poly-PR can also increase the levels of nuclear paraspeckles by direct interaction with paraspeckle proteins and RNA.[68] Given these findings, disruption of protein LLPS is considered as one of the major toxicity mechanisms of arginine-rich DPRs toxicity.

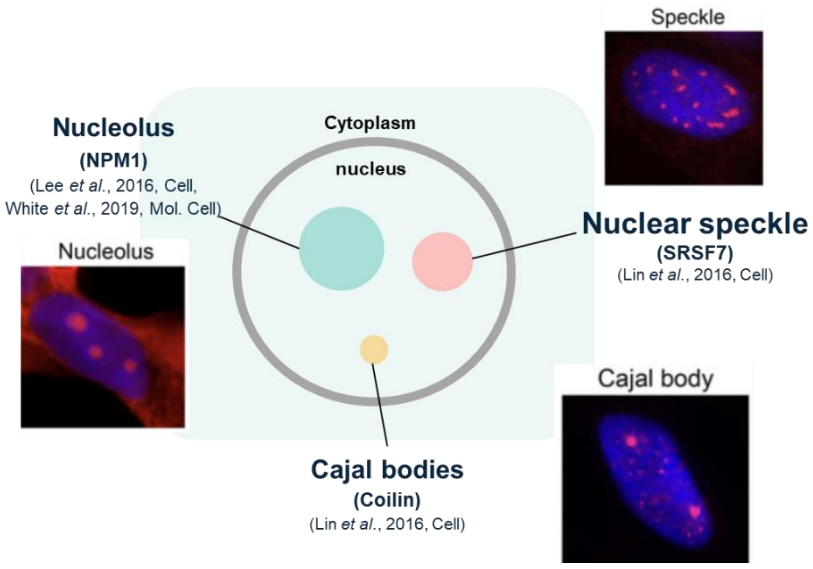

Figure 3. Arginine-rich dipeptides disrupts LLPS of various LCD-rich proteins (for example- NPM1, SRSF7, coilin).[63] Adapted from Lee et al., 2016, Cell, An et al., 2021, BBA – Biomembranes

1.2 TAR-DNA binding protein (TDP-43) is a pathological protein in ALS which also contains LCD

TAR-DNA binding protein 43 (TDP-43) is an RNA-binding protein with low-complexity domains (LCDs), which allows it to undergo liquid-liquid phase separation,

doi:10.6342/NTU202500138

forming dynamic assemblies crucial for cellular organization.[69] Due to the presence of two RNA recognition motifs (RRM1 and RRM2), it can interact with DNA/RNA to regulate transcription and translation of genes.[70] The presence of nuclear localization signal (NLS) at the N-terminal and nuclear export signal (NES) in the RRM2 domain of the protein helps in the shuttling of TDP-43 from nucleus to cytosol and *vice-versa*[71] (Figure 4).

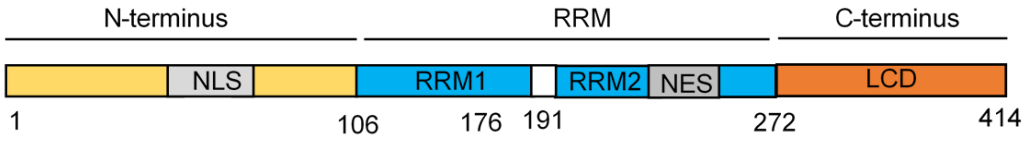

Figure 4. TDP-43 Protein Sequence. TDP-43 protein structure showing N-terminal, C-terminal, RNA recognition motif (RRM1, RRM2), Nuclear export signal (NES) and nuclear localization signal (NLS) domain.

In particular, RRM1 domain has strong affinity to bind with UG-rich single-stranded RNA and these RRM conserved regions play a key role in nucleic acid recognition.[72,73] The function of RRM2 remains obscure and is thought to play a role in organization of chromatin,[74] TDP-43 dimerization.[75] C-terminal domain of TDP-43 is crucial for the interaction with other proteins.[76,77] Due to its multiple interactions, TDP-43 helps in transcriptional regulation, splicing regulation, micro-RNA processing, regulation of subcellular localization of RNA, their translation and decay.[78] However, in ALS patients, nuclear to cytoplasmic mislocalization of TDP-43 and their aggregation in motor neurons is considered to be the major hallmark of ALS.[79] TDP-43 contains six "steric zipper" regions that give rise to irreversible pathogenic amyloid fibrils, while four "low-complexity aromatic-rich kinked segments" contribute to the formation of reversible aggregates.[80] The irreversible

doi:10.6342/NTU202500138

cytoplasmic aggregates of TDP-43 sequesters different RNA-binding proteins and RNA resulting in disruption of cellular processes and cytotoxicity.[81,82] Nuclear to cytoplasmic mislocalization of TDP-43 leads to loss of its normal function causing cellular toxicity.[83]

1.2.1 TDP-43 undergoes phase separation

The presence of intrinsically disordered region in the C-terminus of TDP-43 allows its phase separation in both the nucleus and cytosol.[69,84,85] Under physiological condition, TDP-43 phase separate to form liquid-like droplets called nuclear condensates (NCs).[84] The N-terminal domain of TDP-43 interacts with each other to form dimer or oligomer which facilitates phase separation.[86] However, studies have shown that different factors, like genetic mutations, stress, leads to the transformation of these liquid-like condensates into aggregate, the process known as phase transition.[84,87-89] For example, under oxidative stress the formation of stress granule in cytosol requires TDP-43 and prolonged stress reduce TDP-43 protein level causing dysfunctional stress granule.[90]

In nucleus, TDP-43 undergoes phase separation in response to different kinds of stress and alleviates cytotoxicity in cell and drosophila.[84] It is hypothesized that by increasing the local concentration of the protein, LLPS may alter the soluble state of TDP-43 to its aggregated form.[91] Furthermore, defective LLPS might cause mislocalization of TDP-43 by affecting its nucleocytoplasmic transport.[92] Therefore, understanding the mechanisms governing TDP-43 phase separation and aggregation is crucial for developing therapeutic strategies aimed at mitigating its pathological effects in ALS and FTD. Several cellular modulators, including RNA and chaperones, have been identified as key components that

doi:10.6342/NTU202500138

plays role in maintaining the liquid-like property of TDP-43 LLPS.[93,94] The following sections will cover both RNA and chaperones.

1.2.2 Role of *NEAT1* in TDP-43 LLPS

There are various cellular components that contribute in maintaining the liquid-like property of TDP-43 protein. Due to the presence of RNA recognition motifs in its sequence, TDP-43 phase separation depends upon its interaction with different kinds of RNA. For example, total RNA reduced phase separation of TDP-43 *in vitro.* However, in the same system, the addition of *NEAT1* long non-coding RNA (lncRNA) enhanced TDP-43 condensate formation.[84] In addition to TDP-43, *NEAT1* can also promote the LLPS of paraspeckle proteins, including FUS and NONO. By interacting with their IDR or LCD region, *NEAT1* enhances their weak multivalent interactions, a hallmark of phase separation.[95] The activity of *NEAT1* in promoting LLPS is often length and concentration-dependent. Out of its two isoforms, total (*NEAT1_1+ NEAT1_2*) and long form (*NEAT1_2*), the latter is particularly important for robust phase separation, as its extended sequence offers numerous binding sites for protein interactions.[96] Furthermore, when *NEAT1* or protein levels surpass a threshold, phase separation occurs, leading to droplet formation. This concentration-dependence mirrors the dynamic regulation of paraspeckles in cells.[96] In cellular model, TDP-43 co-phase separate with *NEAT1* RNA to form TDP-43 nuclear condensates.[84] Increase in the levels of *NEAT1* and enhanced colocalization with TDP-43 in spinal motor neurons of early phase ALS patients suggests strong link of *NEAT1* and ALS progression.[97,98] Out of the five *C9ORF72* encoded dipeptides, *NEAT1* upregulation has been observed upon expression of poly-PR dipeptide.[68] This may hint cross-talk of *NEAT1*

doi:10.6342/NTU202500138

positive TDP-43 condensates with poly-PR dipeptide and further aberration of TDP-43 phase separation.

1.2.3 HSP70 Chaperones TDP-43 LLPS

Similar to RNA, molecular chaperones play a crucial role in the regulation of phase separation of different proteins under both physiological conditions and upon stress. By interacting with LCD-rich proteins like TDP-43, FUS, and hnRNPA1, HSP70 prevents the phase transition of their droplets from liquid-like to solid-like or gel-like states, maintaining the dynamic, reversible nature of biomolecular condensates.[99] By recognizing the exposed hydrophobic regions of phase-separating proteins via its ATP-dependent binding and release cycles, HSP70 can effectively modulate protein-protein interactions that drive LLPS.[100] This activity is particularly important in vitro, where HSP70 prevents the pathological transition of droplets from a liquid-like to a gel-like or solid state, a hallmark of protein misfolding diseases. Furthermore, HSP70 collaborates with co-chaperones, such as HSP40 and HSP110, to enhance its disaggregation activity, ensuring that protein condensates remain functional and reversible.[100] The concentration-dependent effects of HSP70 in regulating LLPS have also been demonstrated, with low concentrations stabilizing droplets and higher concentrations leading to their disassembly.[99] In 2014, John et al. showed that heat shock induced TDP-43 condensate aggregation is modulated by heat shock protein 40 or 70 (HSP40/ 70) family of chaperones.[101] Colocalization of HSP70 has been observed in RNA deficient “anisosomal” condensates of TDP-43 to maintain the liquid-like property of TDP-43 through its ATP-dependent activity.[85] Upon arsenite stress, similar HSP70 colocalization with TDP-43 NCs and fluidity maintenance were observed,[102] suggesting the important role

doi:10.6342/NTU202500138

of HSP family chaperones in TDP-43 LLPS. These mechanisms highlight the essential role of HSP70 in preserving cellular proteostasis and inhibiting the development of toxic aggregates linked to neurodegenerative disorders, including ALS and frontotemporal dementia.

1.3 Motivation of the study: TDP-43 Nuclear Condensation in *C9ORF72* ALS

Arginine-rich dipeptides are known to interact with low-complexity domain rich proteins, perturbing their phase separation.[42] However, it remains unclear whether poly-PR and poly-GR dipeptides affects the condensation property of TDP-43 in the nucleus. As these arginine-rich dipeptides are translated in the *C9ORF72* ALS patients, their short-term and long-term presence in the brain may change their toxicity pathway. Therefore, in this study we aim to investigate the LLPS of TDP-43 protein in the nucleus upon different time points of the dipeptide stress. Here, we used the transient (4 hours) and prolonged (12 hours) treatment of arginine-rich dipeptides comparing their effect on TDP-43 LLPS. In addition, given that the phase separation of TDP-43 is modulated by *NEAT1* lncRNA and chaperones under various stresse,[84,85,102] our study also explored the involvement of these components in TDP-43 phase separation. By doing so, we aim to deepen our understanding of how time-dependent treatment of arginine-rich dipeptides may contribute to their toxicity through the disruption of TDP-43 LLPS.

doi:10.6342/NTU202500138

2 Material and Methods

2.1 Cell culture

U2OS human osteosarcoma cells (ATCC, HTB-96) were grown in McCoy's 5A medium (Gibco/ThermoFisher) supplemented with 10% heat-inactivated fetal bovine serum (FBS) and 100 U/mL penicillin-streptomycin (Invitrogen). Cultures were maintained at 37°C in a humidified atmosphere containing 5% CO_2.

2.2 Plasmid construction

The eGFP-TDP-43 plasmid was constructed by cloning the full-length TDP-43 cDNA into the pEGFP-C1 vector, a gift from Dr. Pang-Hsien Tu's lab at the Institute of Biomedical Sciences (IBMS), Academia Sinica, Taipei, Taiwan. The Flag-TDP-43 plasmid was assembled in the pCMV-Tag 2B vector, generously provided by Dr. Che-Kun James Shen's lab at the Institute of Molecular Biology (IMB), Academia Sinica. The PR100-eGFP and GR100-eGFP plasmids were developed using the pEGFP-N1 vector and kindly supplied by Dr. Daisuke Ito from Keio University. Additionally, the mCherry-TDP-43 plasmid was created by replacing the eGFP coding sequence in the eGFP-TDP-43 construct with an mCherry cDNA fragment. The primer sequences used for this modification are as follows:

F: 5' – GCATACCGGTATGGTGAGCAAGGGCGAGG –3'

R: 5' – CAGTGAGCTCCTTGTACAGCTCGTCCATGC –3'

mCherry-HSPA1A was constructed using InFusion Snap Assembly (Takara Bio) and integrated into a custom vector that fuses mCherry at the C-terminus. The coding region for HSPA1A was amplified from a U2OS cDNA library, which was generated using the

doi:10.6342/NTU202500138

SuperScript III First-Strand Synthesis System (Thermo, 18080051). The primer sequences employed in this process are as follows:

Fragment1_ F: 5' – TCAgATCTCgAgCTCAAgCTTATggCCAAAgCCgCggCg –3'

Fragment1_ R: 5' – CgTCgCgCAgAgCCTTCTCCACgggCTCC –3'

Fragment2_F: 5' – ggAgAAggCTCTgCgCgACgCCAAgCTgg –3'

Fragment2 R: 5' – TTATCTAgATCCggTggATCCCTAATCTACCTCCTCAATggTgggg – 3'

All plasmids used in this study were verified to be error-free through sequencing.

2.3 Cell seeding and plasmid transfection

U2OS cells were plated at 8×10^4 cells per well density in a 12-well plate or a glass-bottom dish. After incubating overnight, the cells were transfected transiently with the above specified plasmids using Lipofectamine™ 3000 reagent (Invitrogen) in Opti-MEM (Invitrogen), following the manufacturer's instructions. The plasmid to P3000 to Lipofectamine 3000 ratio was maintained at 1:1:1. Subsequent peptide treatments were carried out after 4 hours or 12 hours, depending on the experiment, following an overnight or 5-hour transfection, respectively. For performing *NEAT1* knock down experiments, U2OS cells were seeded at 4×10^4 cells per well density in a 12-well plate. After incubating overnight, *NEAT1* specific and control siRNAs from Integrated DNA Technology were transfected at a concentration of 20 nM per well using Lipofectamine™ RNAiMax Transfection Reagent (Invitrogen) according to the manufacturer's guidelines. The siRNA was allowed to incubate for about 24 hours before proceeding with eGFP-TDP-43 transfection and peptide treatment. For the overexpression of PR_{100}-eGFP or GR_{100}-eGFP

doi:10.6342/NTU202500138

plasmids, cells were co-transfected with the aforementioned plasmids and mCherry-TDP-43 for 16 hours, as per manufacturer's protocol.

2.4 Establishment and validation of stable N2a cell line expressing eGFP-TDP-43

Neuroblastoma N2a cells were generously provided by Dr. Yijuang Chern from IBMS, Academia Sinica. The cells were cultured in Dulbecco's Modified Eagle Medium supplemented with 10% FBS and Penicillin/Streptomycin at 37°C in a humidified atmosphere with 5% CO2. On the following day, 1×10^6 cells were seeded in a 10-cm dish, and 10 μg of the eGFP-TDP-43-WT plasmid was transfected as previously described. After 24 hours, the medium was replaced with G418-containing medium (1 mg/ml), referred to as the selection medium, to select for transfected cells. After two weeks of selection, islet-like colonies appeared. Following trypsinization, individual cells were sorted and plated into 96-well plates (200 μl/well of selection medium) using a FACSJazz cell sorter (Becton Dickinson). After approximately 14 days in selection medium, independent GFP-positive cell lines were visually examined, selected, and further expanded.

2.5 Synthesis of arginine-rich dipeptides

Synthetic PR_{20}, GR_{20} and random dipeptides were acquired from Yao-Hong Biotechnology Inc. as lyophilized powder. After receiving, the peptides were dissolved in Milli-Q water and aliquoted into small batched for subsequent treatments to cells. For visualizing both PR_{20} and GR_{20} dipeptide, the peptides were labeled with Alexa Fluor-488.

doi:10.6342/NTU202500138

For the labeling process, $(PR)_{20}C$ was dissolved in 100 mM K2HPO4/KH2PO4 buffer (pH 8.0) to create 1 mM stock solution. Alexa Fluor™ 488 C5 Maleimide (ThermoFisher A10254) was prepared fresh in DMSO to generate a 5 mM stock solution. The peptides and AF-488 stock solutions were mixed to yield a solution with 500 μM $(PR)_{20}C$ and 500 μM AF-488. For labeling $(GR)_{20}C$, the peptide stock solution was prepared at 400 μM in the same buffer, resulting in a working concentration of 200 μM for both $(GR)_{20}C$ and AF-488. This mixture was incubated at 37 °C with shaking at 750 rpm for 3 hours. Labeled peptides were purified using high-performance liquid chromatography (HPLC) with a 1260 Infinity LC system (Agilent, USA) equipped with a C18 reversed-phase semipreparative column (Shiseido, Japan). Gradient separation was achieved by combining buffer A (5% acetonitrile/0.1% TFA/94.9% water) and buffer B (0.1% TFA/99.9% acetonitrile), with a flow rate of 3 mL/min. The molecular weights of the peptides were analyzed using matrix-assisted laser desorption/ionization (MALDI) mass spectrometry (Applied Biosystems, USA), with results showing $(PR_{20})C$-488 calculated at 5884.84 g/mol (found m/z 5887.4) and $(GR_{20})C$-488 calculated at 5083.57 g/mol (found m/z 5086).

Random peptide sequence:

PHGWVKSEDMYKECPNRSVRTALRGLQNSSDQKEVLARIE

2.6 Dipeptides and inhibitor treatment

Peptide Treatment: Aliquots of PR_{20}, GR_{20} and random dipeptides were dissolved in McCoy's 5A medium and applied at a concentration of 5 μM[67] to cells, for a time period of 4 and 12 hours respectively, to eGFP-TDP-43 expressing U2OS cells. For the N2a cell line

doi:10.6342/NTU202500138

stably expressing eGFP-TDP-43, the PR_{20} dipeptide was treated at the same concentration for 12 and 24 hours.

Peptide and Inhibitor Co-Treatment: HSP70 activity was inhibited by mixing the HSP70 inhibitor VER155008 (ApexBio, A4387)[85] to 5 μM of the dipeptides, with final concentration of the inhibitor leading to 50 μM (here referred to as PR_{20} + HSPi) to treat cells.

2.7 Antibodies

The following antibodies were utilized for immunostaining: NPM1 (Santa Cruz, sc-56622), rabbit anti-HSP70 (Proteintech, 10995-1-AP), HSP40 (Cell Signaling, C64B4), HSP90 (Proteintech, 13171-1-AP), pTDP-43 (Cosmo Bio, TIP-PTD-M01A), A11 (Invitrogen, AHB0052), ubiquitin (Abcam, AB134953), Anti-Flag M2 (Merck, F1804-200UG and Sigma, F3165, 1MG), TDP-43 (C-terminal) (Proteintech, 12,892-1-AP), and GAPDH (GeneTex, GTX627408). The fluorescent secondary antibodies used included goat anti-mouse-Alexa Fluor 488 (Invitrogen, A11001), goat anti-mouse-Alexa Fluor 568 (Invitrogen, A11004), goat anti-rabbit-Alexa Fluor 568 (Invitrogen, A11011), and goat anti-rabbit-Alexa Fluor 647 (Invitrogen, A21245).

2.8 Immunocytochemistry and Confocal Images

To observe TDP-43 NCs, cells were cultured in a 12-well plate with glass coverslips and transfected with the above-mentioned plasmids. After treatment, 4% paraformaldehyde (PFA) was used to fix the cells for 10 minutes at room temperature. Following washing with PBS, 0.5% Triton X-100 (Bioman Scientific) was used to permeabilize the cells for 15

doi:10.6342/NTU202500138

minutes. To block the background, 5% bovine serum albumin (BSA, Sigma) diluted in 1XPBS was used for one hour at room temperature. Primary antibodies diluted in the blocking solution (0.5% BSA + 0.05% Tween-20 (Sigma) in 1X PBS) was then incubated for overnight at 4°C. Cells were then incubated in secondary antibody diluted in blocking solution for 2-hour incubation at room temperature. Finally, after few PBS washes, nuclear staining was performed with DAPI and images were acquired using 63X oil-immersion objective (numerical aperture 1.4) on a Zeiss LSM780 confocal microscope.

2.9 Proteosome activity assay

U2OS cells were cultured, transfected, and treated with PR20 dipeptides as outlined above. Four hours post-treatment, the cells were collected using ice-cold PBS and lysed in PBS containing 0.05% Tween 20 (Spectrum Chemical MFG CORP, P0132). Insoluble materials were removed by centrifugation at 15,000g for 10 minutes at 4°C. The resulting clear supernatant was transferred to a fresh tube and used to measure proteasome activity using a kit (Abcam, ab107921). Assays were performed following the manufacturer's instructions and analyzed at 37°C using a microplate reader (PerkinElmer, EnSpire 2300 MultiMode).

2.10 Immunofluorescence followed by RNA fluorescence in-situ hybridization (IF-RNA-FISH)

To simultaneously visualize HSP70 and *NEAT1*, cells were seeded onto glass coverslips in a 12-well plate and transfected with the eGFP-TDP-43 plasmid. After various treatments, the cells were fixed with 4% paraformaldehyde (PFA) for 15 minutes and

doi:10.6342/NTU202500138

permeabilized with 0.2% Triton X-100 for 30 minutes at room temperature. After PBS washes, cells were incubated with diluted primary antibodies in blocking buffer for one hour at room temperature, followed by a one-hour incubation with diluted secondary antibodies. Subsequently, cells were washed with Wash Buffer A (Stellaris, SMF-WA1-60, Biosearch Technologies) and hybridized with a diluted *NEAT1* probe (Stellaris FISH probe for human *NEAT1*, 5' segment, SMF-2036-1, or mouse *NEAT1*, 5’ segment, SMF-3009-1, Biosearch Technologies) in hybridization buffer (Stellaris, SMF-HB1-10, Biosearch Technologies) at 37°C for 4–16 hours. Cells were then washed with Wash Buffer B (Stellaris, SMF-WB1-20, Biosearch Technologies) for 5 minutes and stained with DAPI for nuclear visualization. Coverslips were mounted with ProLong™ Diamond Antifade Mountant (Invitrogen), and confocal microscopy was used to capture images.

2.11 Fluorescence recovery after photobleaching (FRAP) analysis

Cells were grown on 35 mm glass-bottom dishes and transfected with the eGFP-TDP-43 plasmid. To induce the formation of TDP-43 nuclear condensates (NCs), the cells were treated with the PR20 dipeptide. Fluorescence recovery after photobleaching (FRAP) assays were performed using the bleaching mode of the Zeiss 710 Confocal Microscope to assess the properties of TDP-43 NCs. Individual NCs were selected and photobleached using a 405 nm laser at 100% power for approximately 5 to 15 iterations. Post-bleaching, time-lapse images were captured over ~70 cycles to track fluorescence recovery, which was quantified by normalizing the background intensities for each field.

doi:10.6342/NTU202500138

2.12 Time-lapse imaging

Cells were seeded onto a 35 mm glass-bottom dish and co-transfected with eGFP-TDP-43 and mCherry-HSPA1A plasmids. Six hours after transfection, the cells were treated with either PR_{20} alone or PR_{20} combined with HSPi, followed by a further 2-hour incubation. Time-lapse imaging was performed using a Nikon TiE microscope, capturing images every 10 minutes over a 2- to 11-hour treatment period. During imaging, live cells were maintained at 37°C in a 5% CO_2 environment.

2.13 RNA isolation and quantitative real-time polymerase chain reaction (qPCR)

Cells were plated in a 12-well plate and co-transfected with either siRNA and eGFP-TDP-43 or solely with the eGFP-TDP-43 plasmid. RNA was extracted using TRIzol (Ambion) following the phenol-chloroform method. Reverse transcription to synthesize cDNA was carried out using the Superscript IV reverse transcriptase kit (Invitrogen/Thermo Fisher Scientific) on a Biometra T3000 thermocycler. Real-time PCR was performed to assess the relative fold changes of both isoforms of *NEAT1* (*NEAT1_1* + *NEAT1_2*; Total, *NEAT1_2*; long form) on an Applied Biosystems thermocycler, utilizing PowerTrack™ SYBR™ Green Master Mix (Applied Biosystems) according to the manufacturer's guidelines. GAPDH mRNA was used as an internal control to normalize the *NEAT1* mRNA levels. Primer pairs for the target RNAs were designed based on human RNA sequences as follows:

doi:10.6342/NTU202500138

Total *NEAT1_1 + NEAT1_2*:

F: 5’ – CAGGAGCTGGAAGTCTTAGAAA – 3’

R: 5’ – CCAGAAGAGCCCATCTAATCTC –3’

Long form *NEAT1_2*:

F: 5’ – TTCTGCTTTCTGCCCATGTA – 3’

R: 5’ – CAACCACAACAGGTGGATTATTT –3’

GAPDH:

F: 5’ – AGCCTCAAGATCATCAGCAAT –3’

F: 5’ – GTCATGAGTCCTTCCACGATAC –3’

2.14 Time Domain fluorescence lifetime imaging

To investigate the FRET efficiency (E_{FRET}) of oligomers within TDP-43 nuclear condensates (NCs), cells were plated on a 35 mm glass-bottom dish and co-transfected with eGFP-TDP-43 and mCherry-TDP-43 plasmids. Following treatment, live cells were observed using an oil-immersion objective [Nikon Plan Apo 100 × /(N.A) 1.4]. The eGFP-TDP-43 excitation sources were from 488 nm (5 mW) sub-nanosecond modulated pulsed laser operating at a fundamental frequency of 20 MHz, controlled by ISS VistaVision software (ISS Inc., Champagne, IL). Photon counts from eGFP-TDP-43 were collected using a GaAs photomultiplier tube (PMT) equipped with an EM1 filter (530/43 nm bandpass filter). To precisely obtain the lifetime value, the system was calibrated by measuring fluorescein (a

doi:10.6342/NTU202500138

fluorophore with a single exponential lifetime around 4 ns in ddH_2O) every time before the measurement.

2.15 FLIM-FRET Data analysis

The fitting method used for analyzing the FastFLIM images was adapted from the "Experimental" section of a previous publication.[103] For the “frame” lifetime fitting model, the lifetime of each pixel in the FastFLIM images (Figures 13A–D) was directly calculated using ISS Software VistaVision, and these values were then converted into E_{FRET} maps (Figures 13A’–D’). By applying a threshold to the photon counts of eGFP-TDP-43, we identified the condensate lifetime in the highlighted pixel regions (Figures S4A’–D’). To determine the lifetime of TDP-43 oligomers within the condensates, the lifetime of eGFP-TDP-43 monomers was fixed at 2.6 ns (the known lifetime of eGFP), allowing us to fit the oligomer lifetimes using a two-exponential frame fitting model. The per-pixel lifetime images were then transformed into per-pixel FRET images using the formula $E_{FRET} = \frac{\tau_D - \tau_{DA}}{\tau_D} = 1 - \frac{\tau_{DA}}{\tau_D}$, where τ_D represents the donor lifetime of GFP alone and τDA indicates the lifetime of the oligomers. These images were exported as an Excel file to calculate the average FRET efficiency (Figure 13E). To fairly assess the E_{FRET} of oligomers, U2OS cells expressing eGFP-TDP-43 were randomly selected. All lifetime values in this study were meticulously fitted within an acceptable range, ensuring a reasonable chi-square value (χ^2).

2.16 Cell Viability assay

Cells were plated in a 12-well plate and co-transfected with either siRNA and eGFP-TDP-43 or solely with the eGFP-TDP-43 plasmid. Following peptide treatment, 100 μL of

doi:10.6342/NTU202500138

lysis buffer was added to specific wells designated as high control (HC), while untreated wells served as low control (LC). From each treated and untreated well, 100 µL of supernatant was transferred to a 96-well plate, followed by the addition of 100 µL of LDH buffer. After a 30-minute incubation, the reaction was stopped with 50 µL of stop solution, and absorbance was measured at 490 nm using an EnSpire multimode plate reader (PerkinElmer). The percentage of LDH release was then calculated using the following formula:

$$\%\ LDH\ release$$

$$= \left(\frac{(Measured\ absorbance\ in\ treated\ group - \ Measured\ Absorbance\ in\ LC)}{(Measured\ absorbance\ in\ HC - \ Measured\ Absorbance\ in\ LC)} \right) X100$$

2.17 Filter Trap assay

U2OS cells were plated at a density of 1×10^5 cells per well in a 6-well plate. The cells were then transfected with the eGFP-TDP-43 plasmid as previously described and incubated overnight. Following this, the cells were treated with the PR_{20} peptide for either 4 or 12 hours. After incubation, the transfected cells were lysed using RIPA buffer containing a protease inhibitor (Roche) and sonicated on ice for 10 seconds. The cell extracts were centrifuged at 14,000 rpm for 10 minutes at 4 °C, and the protein concentration was determined using a bicinchoninic acid (BCA) assay. For the filter trap assay, 200 µL of the sample (equivalent to 50 µg of total protein) was passed through Amersham™ Nitrocellulose (NC) membranes (0.1 µm pore size, GE Healthcare) using a 48-well slot-blot apparatus. The oligomerized eGFP-TDP-43 retained on the NC membrane was then immunoblotted with the A11 antibody (1:2000) and a GAPDH loading control (1:5000) overnight at 4 °C. After

doi:10.6342/NTU202500138

washing with 0.1% PBST, the membranes were incubated with HRP-conjugated secondary antibodies at 4 °C for 4 hours. The blots were washed again and developed using electrochemiluminescence (ECL, Millipore). Signal visualization was performed using the iBright™ FL1000 instrument (Invitrogen).

2.18 Western blot analysis

U2OS cells were seeded at a density of 1×10^5 cells per well in a 6-well plate. After overnight transfection and a 12-hour treatment with the PR_{20} peptide, the cells were lysed using RIPA buffer supplemented with protease inhibitors and then sonicated. Protein concentrations were determined using a BCA assay. For electrophoresis, 20 μg of protein was loaded onto a 12% Tris–glycine SDS-PAGE gel. Separated proteins were transferred onto a PVDF membrane (Millipore). The membranes were blocked for at least 1 hour with 5% bovine serum albumin (BSA, Sigma) in 0.1% PBST. After blocking, the blots were incubated overnight at 4 °C on a shaker with primary antibodies, including p-TDP-43 (pS409/410) (1:1000), TDP-43 (C-terminal) (1:1000), and GAPDH (1:5000), diluted in 2–5% BSA. Following washes with 0.1% PBST, the membranes were incubated with HRP-conjugated secondary antibodies for 2 hours at room temperature. After additional washes, the blots were developed using electrochemiluminescence (ECL, Millipore), and signals were visualized with the iBright™ FL1000 instrument (Invitrogen).

2.19 Image quantification and statistical analysis

Puncta counts and Pearson correlation coefficients (PCCs) were analyzed using Fiji ImageJ. Colocalization profiles were also generated using Fiji ImageJ. All statistical analyses were conducted using GraphPad Prism, employing One-way ANOVA with Tukey's multiple

doi:10.6342/NTU202500138

comparisons test, Two-way ANOVA with Tukey's multiple comparisons test, and Unpaired *t*-tests (two-tailed) were used to assess the significance of the data. P values were defined as follows: *p < 0.05, **p < 0.01, ***p < 0.001, and "ns" for non-significant results. Error bars corresponds to standard deviation.

doi:10.6342/NTU202500138

3 Results

3.1 Transient poly-PR stress induces TDP-43 nuclear condensation with reduced fluidity

Several studies have shown that arginine-rich dipeptides impair biophysical properties of proteins like NPM1, G3BP1 eventually perturbing the dynamics of membraneless organelles.[42,64,66] TDP-43 is an important ALS-associated protein that undergoes nuclear phase separation in response to various kinds of stress.[57,84,102,104] However, the impact of arginine-rich dipeptides on LLPS of TDP-43 in the nucleus upon arginine-rich DPR treatment remains unclear. To investigate the effect of arginine-rich dipeptides on LLPS of TDP-43 in the nucleus, we examined TDP-43 nuclear condensates (NCs) number upon 5 μM of synthetic PR_{20} and GR_{20} dipeptide treatment for 4 hours. We monitored the phase separation behavior of overexpressed eGFP-TDP-43 protein in U2OS cells by applying confocal microscopy.

Our data showed that cells with no treatment of the dipeptides, that is in the control group, possessed fewer TDP-43 NCs (upper panel in Figure 5A). While treatment with PR_{20} dipeptide induced more GFP-TDP-43 NCs formation (middle panel in Figure 5A) than GR_{20} (lower panel in Figure 5A). The statical analysis revealed enhanced TDP-43 NCs formation only in PR_{20} treated group compared to both the control and GR_{20} groups (Figure 5B). To address the potential concern of GFP dimerization, we recapitulated this phenotype in other flag-TDP-43 overexpression system and results showed a significant increase of Flag-TDP-43 NCs number upon PR_{20} treatment but neither in control nor GR_{20} groups (Figure 5C, 5D).

doi:10.6342/NTU202500138

One of the important property of the condensates is their ability of the continuously exchange with the surrounding nucleoplasm,[105] which imparts fluidity/ liquid-like behavior to these condensates. The fluidity of the condensates is widely measured by a fluorescence recovery after photobleaching (FRAP) technique. In FRAP, the GFP expressing condensates were first bleached at 0 s and those bleached NCs are allowed to recover with time. The higher the recovery rate of the condensates, the more is their fluidity. Therefore, we applied FRAP analysis in eGFP-TDP-43 expressing live U2OS cells to measure the NCs fluidity. In the control group, the fluorescence recovery of GFP-TDP-43 NCs was approximately 75% of the pre-bleaching intensity at 75 s (upper panel in Figure 5E), suggesting highly fluidic TDP-43 NCs under physiological condition. However, upon PR_{20} dipeptide treatment, the fluorescence recovery of the condensates decreases to approximately 50% (middle panel in Figure 5E) while GR_{20} treatment did not reduce the recovery (lower panel in Figure 5E). The quantification curve depicted reduced fluorescence recovery in PR_{20} group compared to both the control and GR_{20} group (Figure 5F). These findings indicate that only PR_{20} dipeptide reduce the liquid-like property of TDP-43 NCs.

doi:10.6342/NTU202500138

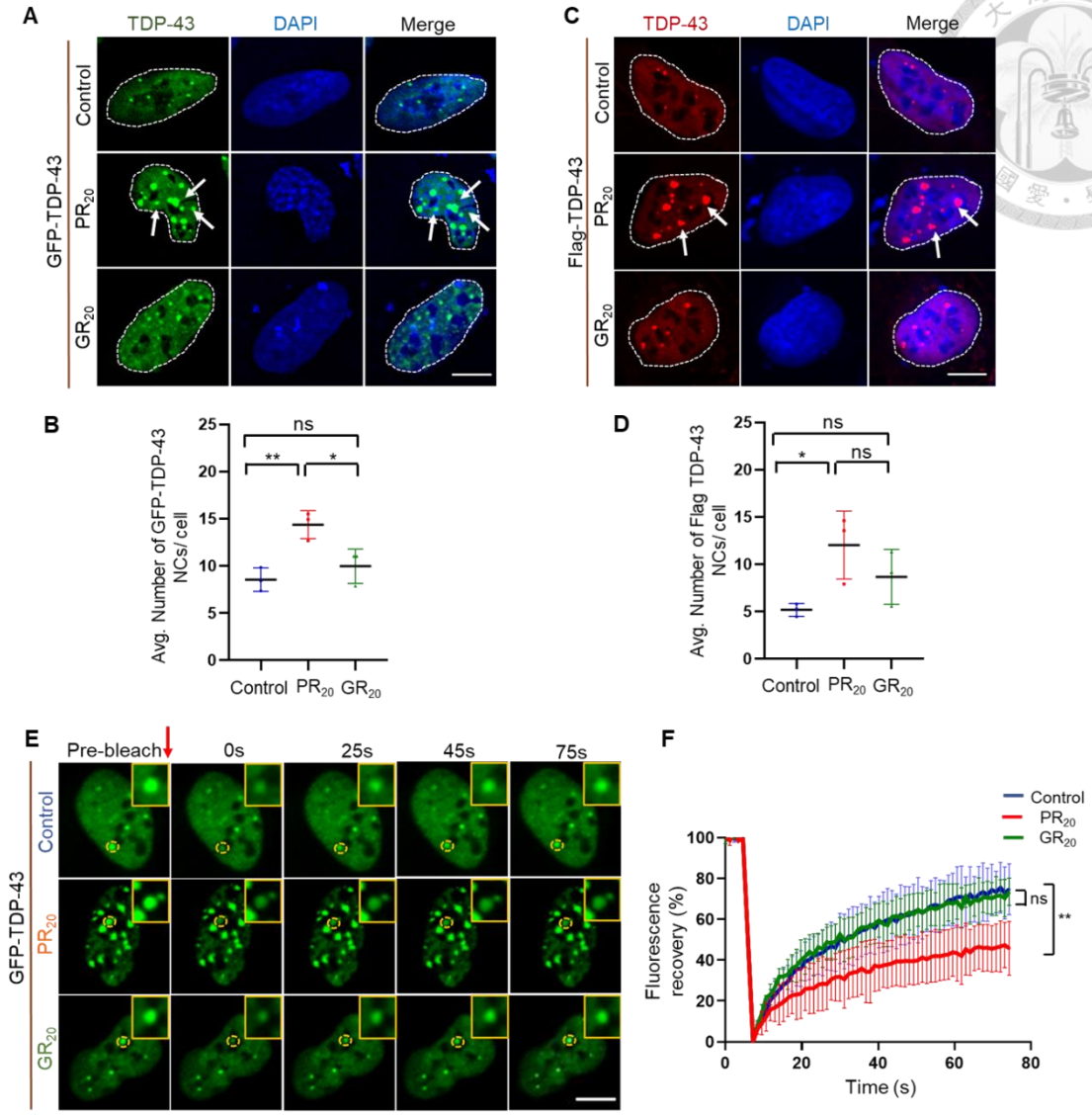

Figure 5. Poly-PR dipeptide promotes phase separation of TDP-43 more than Poly-GR. (A and C) Confocal images representing eGFP-TDP-43 and Flag-TDP-43 nuclear condensates (NCs) upon transient PR_{20} and GR_{20} dipeptide treatment. Arrows show enhanced TDP-43 NCs formation only in PR_{20} treated group. DAPI indicates nuclear labeling. Dashed line represents nucleus. (B and D) Quantification of number of eGFP-TDP-43 and Flag-TDP-43 NCs per cell. n>125 independent cells were pooled and analyzed for counting number of TDP-43 nuclear condensates from three independent peptide treatments (N=3). (E) FRAP images showing fluorescence recovery upon PR_{20} and GR_{20} dipeptide treatment. Circle indicate the bleached puncta. (F) Quantification of fluorescence recovery upon dipeptides

doi:10.6342/NTU202500138

treatment. Error bar corresponds to standard deviation; One-way ANOVA analysis with Tukey's multiple comparison test was used in (B) and (D), Two-way ANOVA with Tukey's multiple comparison test was used in (F) *p<0.05, **p<0.01, ns= non-significant. Scale bars, 10 μm (A, C, E).

3.2 Transient poly-PR stress fails to induce FUS and GFP-NLS nuclear condensation

To check whether other nuclear proteins also under LLPS under poly-PR stress, we also investigated the effect of transient poly-PR stress on nuclear condensation of ALS-associated protein Fused in sarcoma (FUS) and GFP-tagged nuclear localization signal protein (GFP-NLS). The confocal images showed that FUS-GFP NCs did not show any significant increase upon transient poly-PR stress (Figure 6A, 6B). Similar to these observations, transient poly-PR stress did not induce GFP-NLC NCs (Figure 6C), suggesting that the effect of poly-PR stress is specific to TDP-43 protein and is not a general phenomenon associated with any nuclear protein.

doi:10.6342/NTU202500138

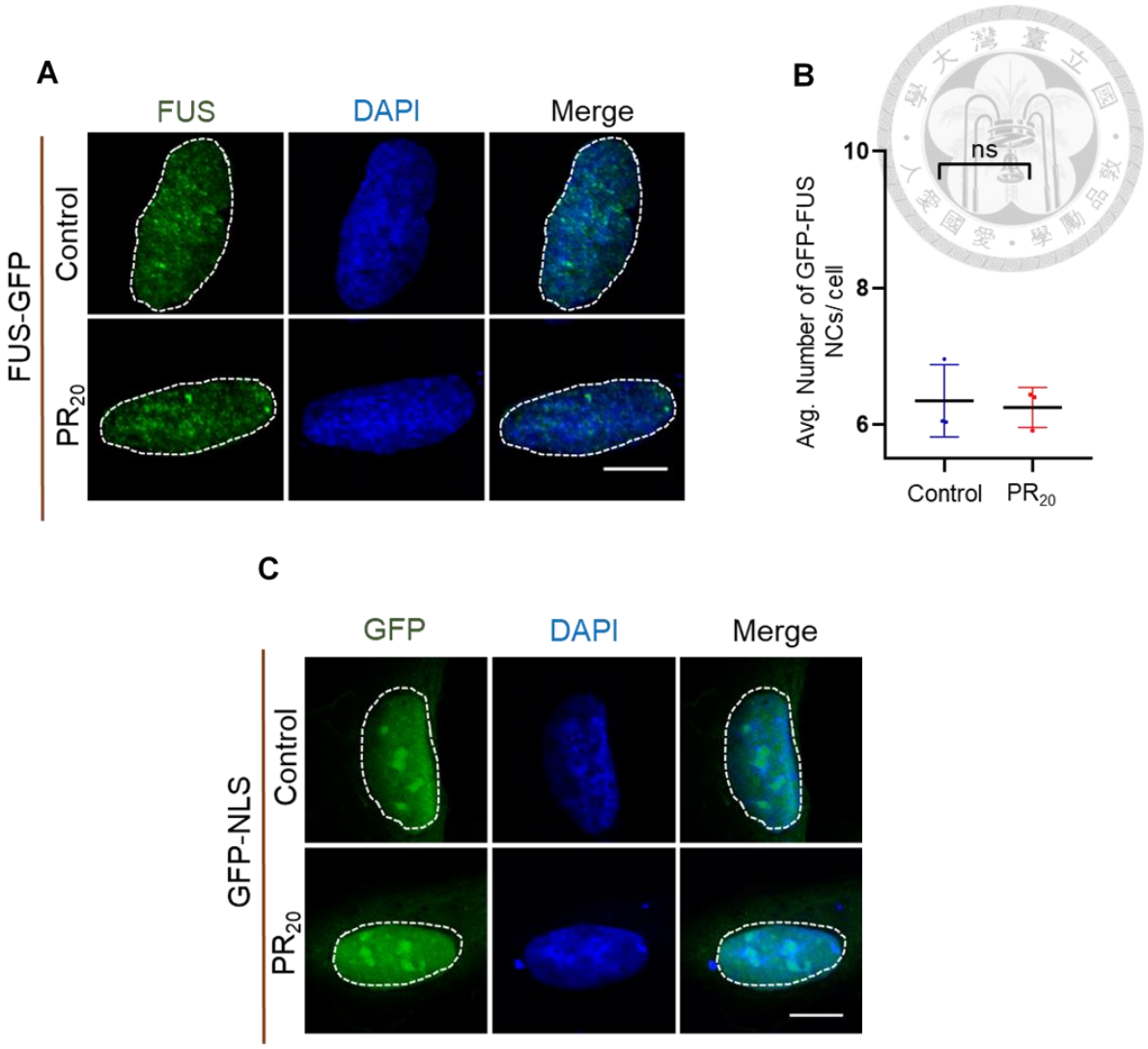

Figure 6. Poly-PR stress did not induce FUS-GFP and GFP-NLS nuclear condensation. (A and C) Confocal images representing of eGFP-FUS and eGFP-NLS nuclear condensates (NCs) upon transient PR_{20} treatment. DAPI represents nuclear labeling. Dashed line shows nucleus. (B) Quantification of number of GFP-FUS NCs per cell in the nucleus. n > 135 independent cells were analyzed from three independent peptide treatments (N = 3). Unpaired *t* test was used in (B); ns= non-significant. Scale bars, 10 μm (A, C).

3.3 Random peptide did not induce TDP-43 NCs

Nuclear condensation of TDP-43 is typically observed in poly-PR but not poly-GR stress. To test whether similar length random peptide sequence will have the similar phenotype effect on TDP-43 nuclear condensation, we transiently treated the cells with

doi:10.6342/NTU202500138

random peptide (sequence provided in the Material and method section). Our data showed that random peptide had no effect on TDP-43 NCs number (Figure 7A, 7B), suggesting TDP-43 nuclear condensation is specific to poly-PR treatment.

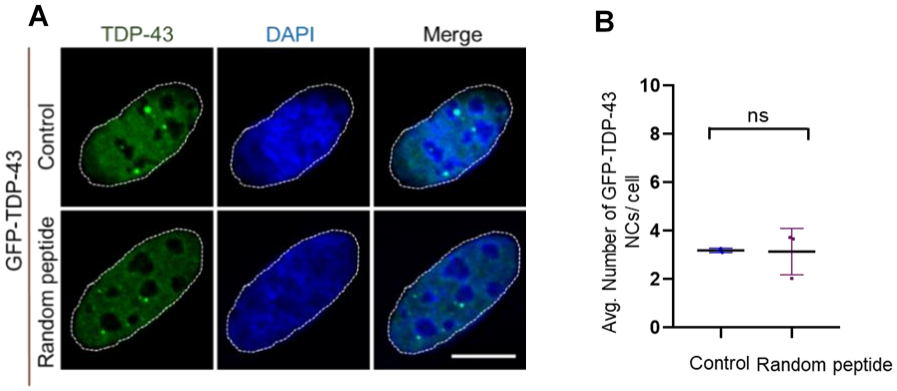

Figure 7. Random peptide did not induce TDP-43 nuclear condensation. (A) Confocal images representing eGFP-TDP-43 NCs upon transient random peptide treatment. DAPI represents nuclear labeling. Dashed line shows nucleus. (B) Quantification of number of GFP-TDP-43 NCs per cell in the nucleus. n > 135 independent cells were analyzed from three independent peptide treatments (N = 3). Unpaired *t* test was used in (B); ns= non-significant. Scale bars, 10 μm (A).

3.4 Nucleolar localized poly-PR indirectly induce TDP-43 nuclear condensation

As we observed increased TDP-43 NCs number upon poly-PR stress, we were interested to explore the localization of TDP-43 NCs with respect to the dipeptide repeats. To achieve this, we treated Alexa fluor-488 labeled PR_{20} dipeptide (PR_{20}-AF-488) and GR_{20} dipeptide (GR_{20}-AF-488) in mCherry-TDP-43 overexpressing U2OS cells. Studies have shown that arginine-rich dipeptides preferentially reside in the nucleolus.[42,66,67] Therefore, we also immunostained the aforementioned treated cells with nucleolar protein NPM1. Consistent with the previous studies, labelled PR_{20} dipeptide localized strongly within the

doi:10.6342/NTU202500138

nucleolus, as they colocalize with NPM1 protein (Figure 8B). Similar to previous observations, only PR_{20} enhanced mCherry-TDP-43 NCs formation (Figure 8B) compared to control (Figure 8A, 8D). It is worth to note that, poly-PR induced TDP-43 NCs did not colocalized with nucleolar occupied poly-PR, as shown in the profiling (Figure 8E), suggesting indirect induction of TDP-43 NCs upon poly-PR stress. Meanwhile GR_{20} dipeptide localized both in the nucleus and cytosol (Figure 8C, 8F) and did not induce mCherry-TDP-43 NCs formation.

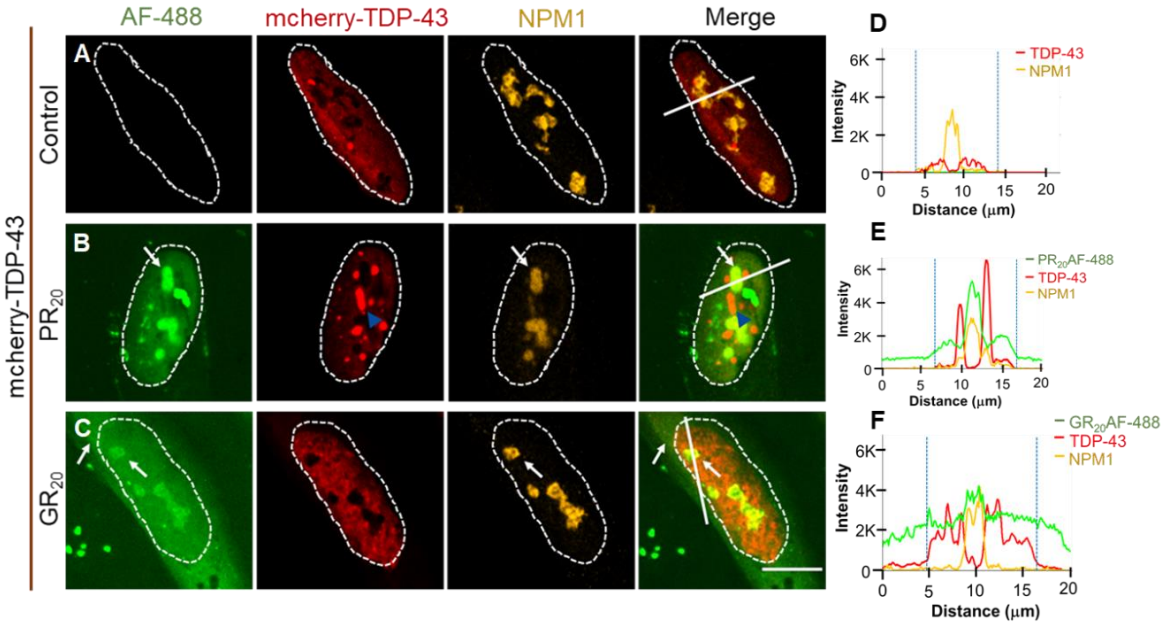

Figure 8. Nucleolar occupied Poly-PR dipeptide indirectly induce TDP-43 nuclear condensation. (A-C) Confocal images of mCherry-TDP-43 NCs treated with 5μM of Alexa-flour-488 labelled arginine-rich dipeptides for 4 hours and immunostained with nucleolar marker, NPM1. White arrows indicate localization of PR_{20} and GR_{20} dipeptide, blue arrows indicate enhanced mCherry-TDP-43 NCs formation in PR_{20} treated group. Dashed line shows nucleus. (D, E, F) Profiling of TDP-43 NCs with labelled PR_{20} and GR_{20} dipeptide and NPM1 along the line drawn in A, B, C respectively. Scale bars, 10 μm (A-C).

doi:10.6342/NTU202500138

3.5 Longer, but not shorter, length dipeptides show similar TDP-43 NCs induction

In order to establish that the poly-PR induced TDP-43 nuclear condensation occurs with different lengths of the dipeptide, we investigated the nuclear condensation of TDP-43 upon longer length arginine-rich dipeptides overexpression. Our data showed that, GFP only group had fewer TDP-43 NCs (upper panel in Figure 9A). Overexpression of PR_{100}-GFP significantly increased the number of mCherry-TDP-43 NCs (middle panel in Figure 9A) compared to GR_{100}-GFP group (lower panel in Figure 9A). Statistical analysis of TDP-43 NCs number showed increase in PR_{100} group compared to both control and GR_{100} (Figure 9B). Of note, longer length poly-PR dipeptide preserved their nucleolar localization while poly-GR localized both in the nucleolus and cytosol (Figure 9A). In addition, TDP-43 NCs did not colocalize with nucleolar occupying poly-PR (middle panel in Figure 9A). These findings confirm that poly-PR indirectly induced TDP-43 nuclear condensation.

doi:10.6342/NTU202500138

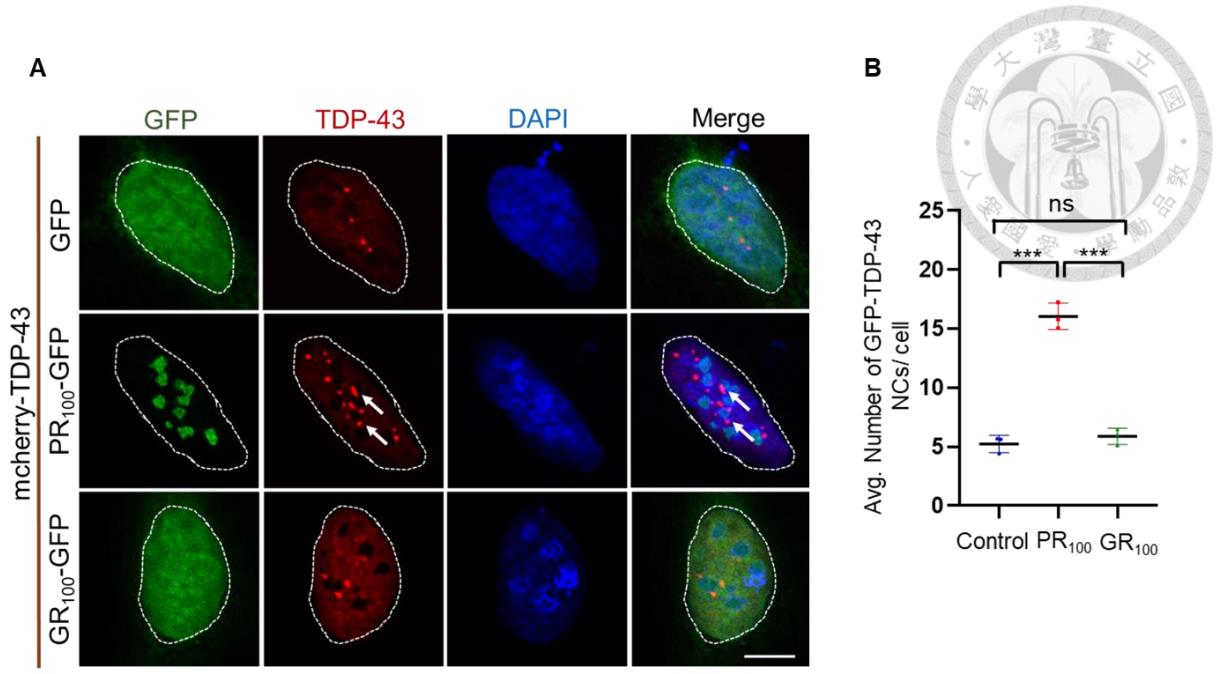

Figure 9. Overexpressed Poly-PR dipeptide indirectly induced TDP-43 nuclear condensation. (A) Confocal images of mCherry-TDP-43 NCs upon 16 hours of PR_{100}-GFP and GR_{100}-GFP overexpression indicate enhanced TDP-43 NCs formation. White arrows represent enhanced mCherry-TDP-43 NCs formation in PR_{100}-GFP group. DAPI for nuclear labeling. Dashed line indicates nucleus. (B) Quantification of number of mCherry-TDP-43 NCs upon dipeptide overexpression. n>145 independent cells were pooled and analyzed for counting the number of TDP-43 NCs from three independent peptide treatments (N=3). Error bar corresponds to standard deviation; One-way ANOVA analysis with Tukey's multiple comparison test was used in (B), ***p<0.001, ns= non-significant. Scale bars, 10 μm (A).

3.6 Nucleolar occupied poly-PR dipeptide did not induce proteasomal stress

There is a notion that proteasomal activity might be compromised in response to disrupted nucleolus.[106,107] To learn whether nucleolar-occupying poly-PR dipeptide causes proteolytic stress by impairing proteasomes, we analyzed the proteasome activity with a fluorogenic assay. Our data showed no significant difference between control and poly-PR

doi:10.6342/NTU202500138

dipeptide-treated group (MG132-treated groups were served as negative control) (Figures 10A and 10B), suggesting that poly-PR induced TDP-43 nuclear condensation is not linked to proteolytic stress.

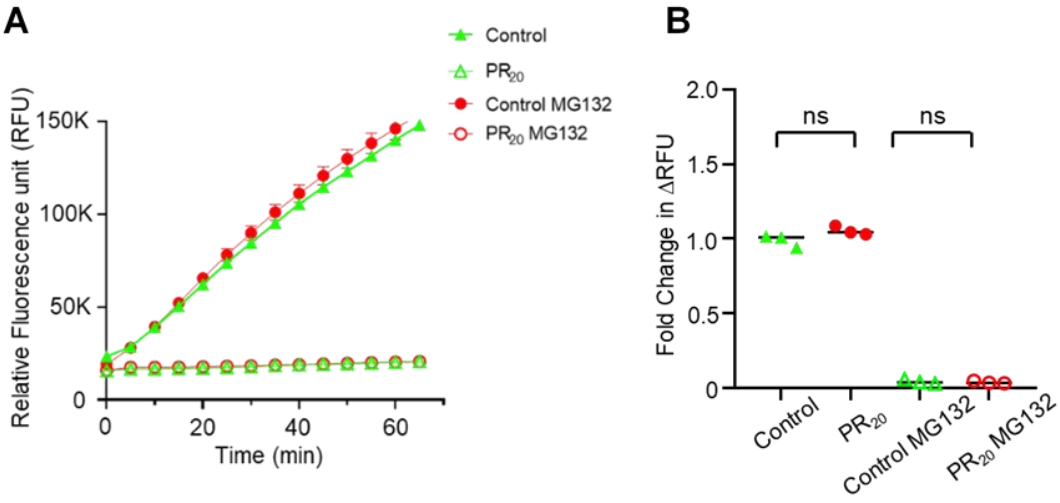

Figure 10. Poly-PR induced TDP-43 nuclear condensation is not correlated with proteasomal stress. (A) Fluorogenic assay to evaluate proteosome activity of GFP-TDP-43 expressing cells upon poly-PR dipeptide treatment. Relative fluorescence unit (RFU) over time upon PR_{20} treatment along with the control group. Co-treatment of MG132 (Control MG132 and PR_{20} MG132) serves as negative control. (F) Quantification of normalized fold change in ΔRFU. Error bar corresponds to standard deviation; One-way ANOVA with Tukey's multiple comparisons test was used in (B), ns= non-significant.

3.7 Transient Poly-PR induced TDP-43 NCs colocalize with *NEAT1* RNA and HSP70 Chaperone

Recent studies have shown the role of *NEAT1* long-coding RNA in providing nucleation scaffolds to condense TDP-43 promoting its LLPS and nuclear condensate formation.[84] Of note, out of the five *C9ORF72* encoded dipeptides, only Poly-PR upregulates *NEAT1*.[68] In addition, HSP70 chaperones plays a crucial role in protecting the proteins from

doi:10.6342/NTU202500138

various kinds of cellular stress, maintaining protein homeostasis and preventing their aggregation.[108] Recent studies have shown that HSP70 participate in regulating the liquid-like property of TDP-43 protein, preventing its phase transition.[85,102] Therefore, we utilized immunofluorescence followed by RNA-FISH to investigate whether *NEAT1* and HSP70 participate in Poly-PR induced TDP-43 nuclear condensate formation.

In the control group, partial colocalization of *NEAT1* was observed within GFP-TDP-43 NCs (Figure 11A, 11C) and they Pearson correlation coefficient of around 0.63 (Figure 11E). Upon prolonged PR_{20} treatment, higher colocalization of *NEAT1* within GFP-TDP-43 NCs were observed (Figure 11B, 11D) and the Pearson correlation coefficient was significantly increased to around 0.74 (Figure 11E). Similar to these observations, in the control group HSP70 was not enriched within eGFP-TDP-43 NCs (Figure 11A, 11C) and the Pearson correlation coefficient was approximately 0.4 (Figure 11F). However, in poly-PR treated group, enrichment of HSP70 in eGFP-TDP-43 NCs were observed (Figure 11B, 11D) and the Pearson correlation coefficient was increased to around 0.6 (Figure 11F). Altogether these results suggests that transient poly-PR stress induced TDP-43 NCs colocalize with *NEAT1* and HSP70.

doi:10.6342/NTU202500138

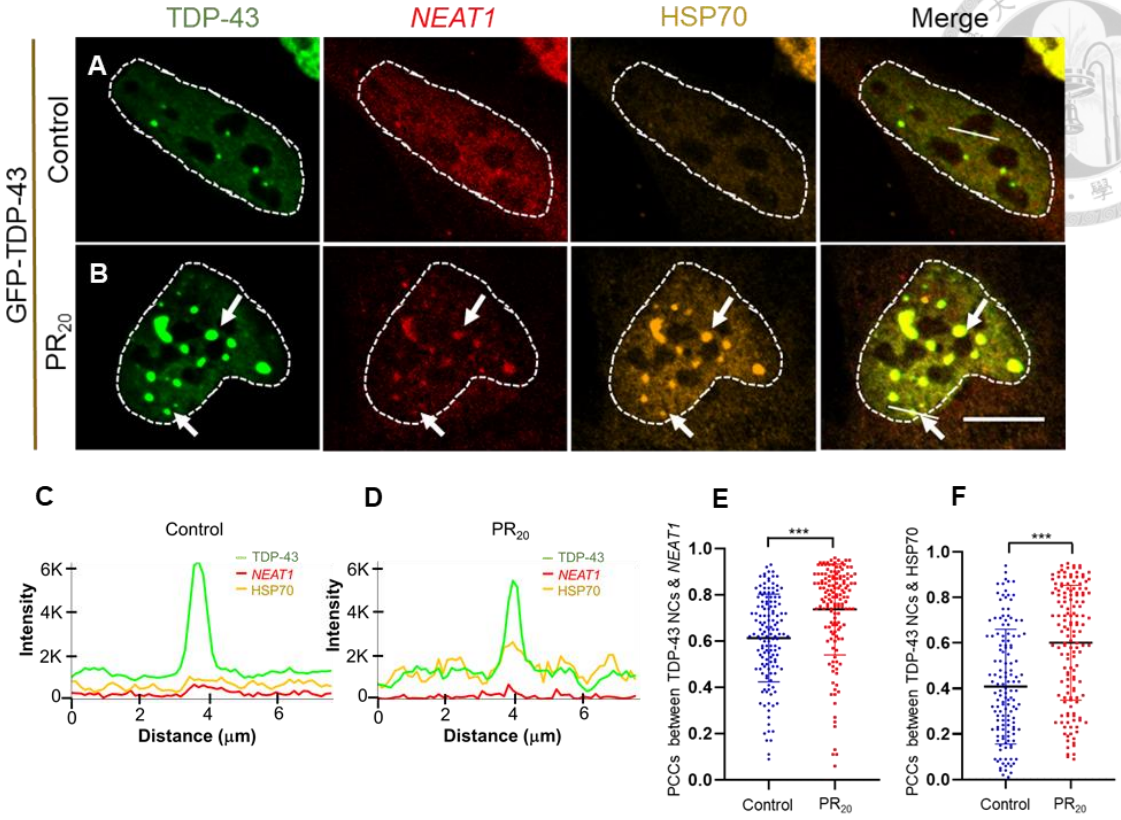

Figure 11. Poly-PR stress induced TDP-43 NCs colocalized with *NEAT1* lncRNA and HSP70 chaperone. (A, B) Confocal images of eGFP-TDP-43 NCs upon transient PR_{20} dipeptide treatment, probed for *NEAT1* lncRNA and immunostained for HSP70 chaperone using I-RNA-FISH. (C, D) Profiling of TDP-43 NCs with *NEAT1* and HSP70 along the line indicated in A and B. (E, F) Pearson correlation coefficients reflect the colocalization of eGFP-TDP-43 NCs with *NEAT1* and HSP70. n>140 independent cells were pooled and analyzed from three independent peptide treatment (N=3). Error bar corresponds to standard deviation; Unpaired *t*-test was used in (E) and (F). ***p<0.001. Scale bars, 10 μm (A, B).

3.8 Other Chaperones and paraspeckle proteins do not colocalize with transient Poly-PR induced TDP-43 NCs

Different classes of heat shock proteins (HSPs) have shown to participate in maintaining the liquid-like property of protein condensates. HSP40 and HSP90 regulate the biophysical properties of FUS and purine condensates respectively.[109,110] We analyzed these

doi:10.6342/NTU202500138

HSPs in poly-PR induced TDP-43 NCs. In the control, TDP-43 NCs did not colocalize with neither HSP40 nor HSP90 (Figure 12A, 12C). In poly-PR group, induced TDP-43 NCs also showed no enrichment for HSP40 or HSP90 (Figure 12B, 12D). In addition to chaperones, we also examined paraspeckle protein (NONO) and its colocalization with TDP-43 NCs. Our results showed that transient poly-PR stress induced TDP-43 NCs did not colocalize with *NEAT1*-positive TDP-43 NCs (Figure 12E-12G). Altogether these observations suggests that only HSP70 participate in poly-PR induced TDP-43 nuclear condensation.

doi:10.6342/NTU202500138

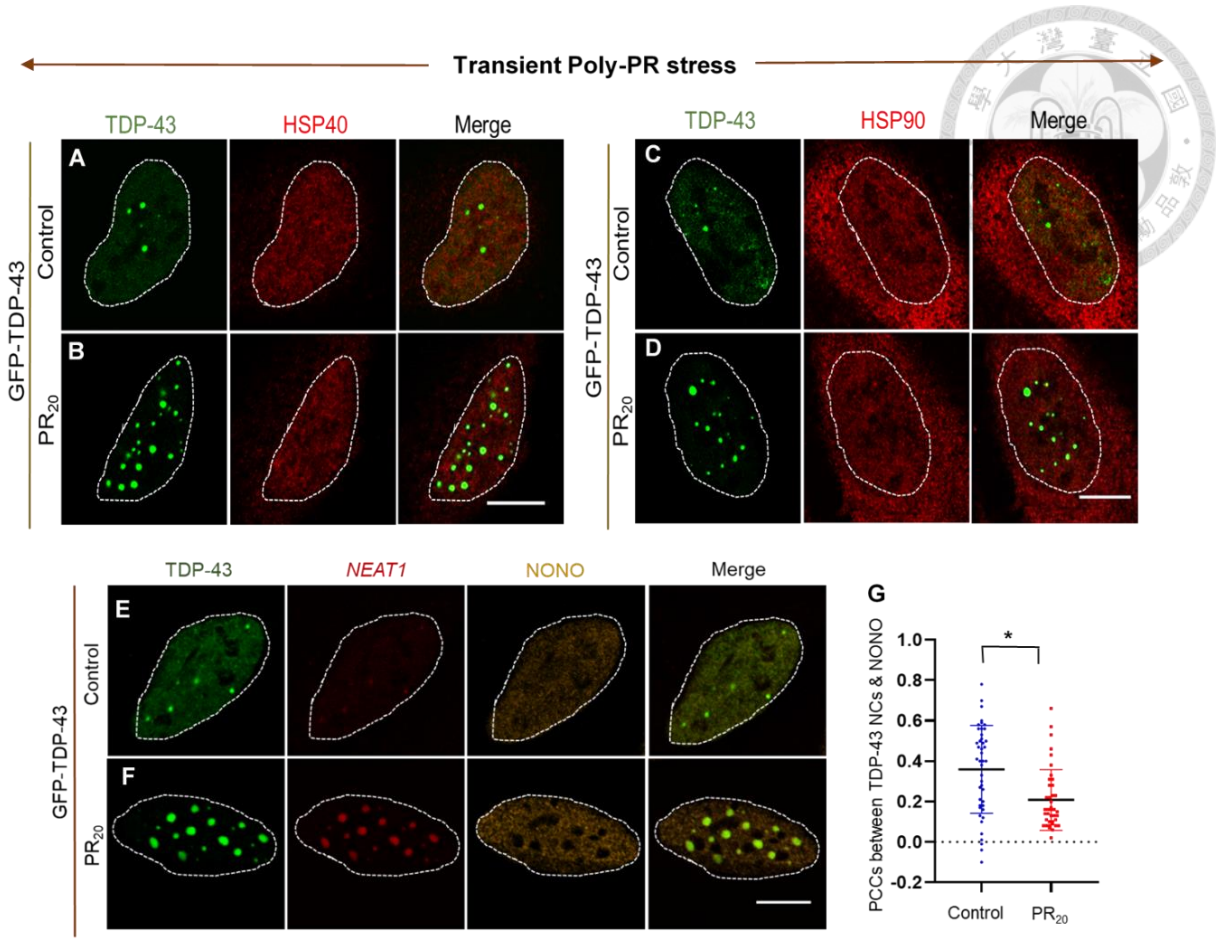

Figure 12. HSP40 and HSP90 chaperones as well as paraspeckle protein (NONO) does not participate in poly-PR induced TDP-43 nuclear condensation. (A-D) Confocal images of eGFP-TDP-43 NCs upon 5μM of PR_{20} dipeptide treatment for 4 hours shows no colocalization with neither HSP70 nor HSP90. Scale bars, 10 μm (A-D). (E, F) Representative images of GFP-TDP-43 NCs upon 5 μM of PR_{20} dipeptide treatment for 4 hours in U2OS cells, co-stained with *NEAT1* lncRNA and NONO by IF-RNA-FISH. Dashed line represents nucleus. (G) Pearson correlation coefficients (PCCs) reflect the low co-localization of GFP-TDP-43 NCs with NONO. n>40 independent cells were analyzed from single peptide treatment. Error bars corresponds to standard deviation; Unpaired t test was used in (G). *$p<0.05$. Scale bar, 10 μm (A-F).

doi:10.6342/NTU202500138

3.9 *NEAT1* promotes TDP-43 nuclear condensation and HSP70 recruitment to NCs under transient poly-PR stress

TDP-43 is a nuclear protein that bind to DNA/ RNA regulating transcription, translation and splicing of various genes[111] which binds preferentially to UG-rich RNA sequences.[98,112-114] *NEAT1* lncRNA has three UG-rich repeat regions[98,115] and analysis of FTLD-TDP patient samples showed enhanced TDP-43 binding to *NEAT1* RNA.[98] Furthermore, invitro data indicate that *NEAT1* promotes TDP-43 LLPS.[84] As TDP-43 NCs were positive for *NEAT1*, we performed *NEAT1* knockdown to explore its function in poly-PR induced TDP-43 NCs formation. To achieve this, we used specific small interfering RNA to knockdown both isoforms of *NEAT1* (*NEAT1_1 + NEAT1_2*; Total, *NEAT1_2*; long-form). The knockdown data showed the depletion of *NEAT1* by less than 50%, as depicted in quantitative polymerase chain reaction (qPCR) results (Supplementary Figure 1).

The results in the control group (siCtrl; without *NEAT1* knockdown) with PR_{20} dipeptide ($+PR_{20}$) treatment showed increase in the number of TDP-43 NCs (Figure 13B) compared to no peptide treatment group ($-PR_{20}$) (Figure 13A). By contrast, knocking down of *NEAT1* (si*NEAT1*) reduced the TDP-43 NCs count both in PR_{20} dipeptide treated group ($+PR_{20}$) (Figure 13D) or the group without dipeptide treatment ($-PR_{20}$) (Figure 13C). The statistical analysis depicted reduction in the number of TDP-43 NCs upon *NEAT1* knockdown (Figure 13I). These findings suggests that *NEAT1* is essential for the formation of TDP-43 NCs under physiological conditions and upon poly-PR stress.

doi:10.6342/NTU202500138

In addition, we also explored the localization of HSP70 chaperone with respect to TDP-43 NCs upon depletion of *NEAT1*. In the control group (siCtrl) with PR_{20} dipeptide ($+PR_{20}$) treatment, colocalization of HSP70 within TDP-43 NCs were observed (Figure 13B, 13F) compared to no peptide treatment group ($-PR_{20}$) (Figure 13A, 13E). By contrast, knocking down of *NEAT1* (si*NEAT1*) prevented the enrichment of HSP70 within these condensates in both the PR_{20} dipeptide treated ($+PR_{20}$) (Figure 13D, 13H) and untreated group ($-PR_{20}$) (Figure 13C, 13G). The statistical analysis confirmed the reduction in Pearson correlation coefficient between TDP-43 NCs and HSP70 (Figure 13J). These findings suggests that *NEAT1* helps in the recruitment of HSP70 to TDP-43 NCs upon transient poly-PR stress.

doi:10.6342/NTU202500138

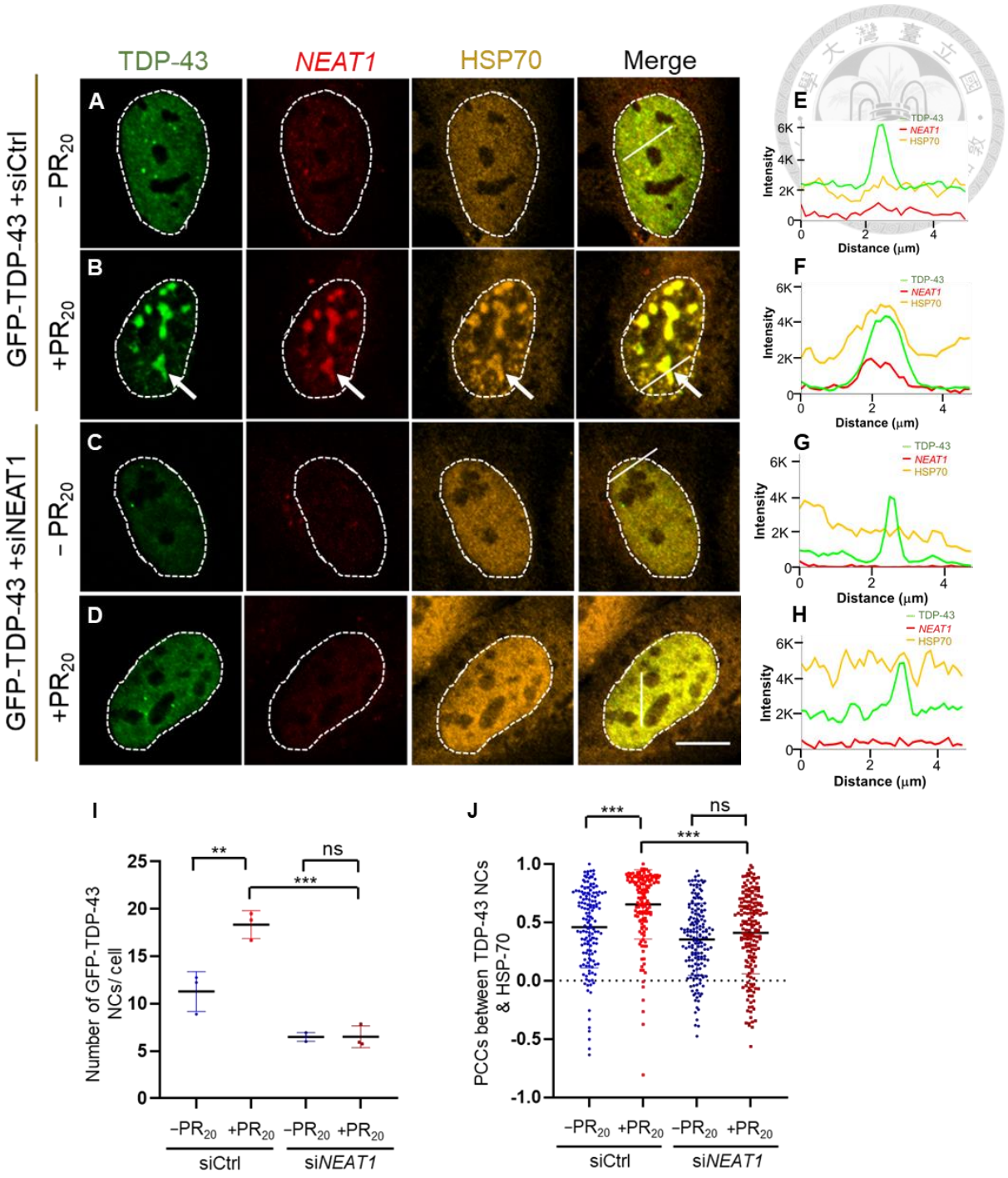

Figure 13. *NEAT1* promotes TDP-43 nuclear condensation and HSP70 recruitment to the condensates under transient poly-PR stress. (A-D) Confocal images of TDP-43 NCs following *NEAT1* knockdown (si *NEAT1*) with or without PR_{20} dipeptide treatment for 4 hours, probed for *NEAT1* lncRNA and immunostained for the HSP70 chaperone using immunostaining and RNA-FISH. (E-H) Intensity profiles of GFP-TDP-43 NCs for *NEAT1*

doi:10.6342/NTU202500138

and HSP70 along the indicated lines in (A-D). The green line represents GFP-TDP-43 NCs, the red line represents *NEAT1*, and the yellow line represents HSP70. (I) Quantification of GFP-TDP-43 NCs following *NEAT1* knockdown. More than 150 independent cells were pooled and counted from three independent peptide treatments (N=3). (J) Pearson correlation coefficients (PCCs) showing the co-localization of GFP-TDP-43 NCs with HSP70 after *NEAT1* knockdown and PR_{20} dipeptide treatment. More than 150 independent cells were pooled and counted from three independent treatments (N=3). Error bars represent standard deviation; One-way ANOVA with Tukey's multiple comparison test was used in (I) and (J). **p<0.01, ***p<0.001, ns = non-significant. Scale bars, 10 μm (A-D).

3.10 HSP70 maintains fluidity of TDP-43 NCs under transient poly-PR stress

Stress induces TDP-43 NCs formation and prolonged exposure to stress reduce the fluidity of these NCs resulting in their phase transition.[84] HSPs functions to refold the misfolded proteins.[116] Analysis of TDP-43 protein interactome revealed that many HSPs can interact with TDP-43.[85,117] Studies have recently showed that HSP70 participate in maintaining the fluidity of TDP-43 NCs upon stress[102] as well as in RNA deficient condition.[85] Our colocalization results show the participation of HSP70 in TDP-43 nuclear condensation (Figure 11). However, whether HSP70 maintains the fluidity of TDP-43 NCs upon poly-PR stress remains unknown.

HSP70 requires ATP hydrolysis to refold misfolded proteins[118] and blocking the ATPase activity leads to its inhibition.[119] Therefore, we used HSP70 inhibitor to impede the activity of HSP70.[120] For confirming whether the localization of HSP70 within the condensates did not alter upon inhibition of HSP70, we performed immunostaining. In the DMSO control group, TDP-43 NCs did not colocalize with HSP70 (Figure 14A, 14D). As

doi:10.6342/NTU202500138

expected, PR_{20} dipeptide treatment induced colocalization of HSP70 within the condensates (Figure 14B, 14E). Similar to poly-PR treated group, co-treatment of HSP70 inhibitor with poly-PR (PR_{20}+HSPi) induced HSP70 enrichment within the condensates (Figure 14C, 14F). Our statistical analysis depicted increased Pearson correlation coefficient between TDP-43 NCs and HSP70 upon both PR_{20} and PR_{20}+HSPi treatment (Figure 14G). These observations confirmed that the inhibition of HSP70 did not change poly-PR induced TDP-43 phenotype.

Next, we conducted FRAP assay to determine the fluidity of TDP-43 NCs upon HSP70 inhibition. In the DMSO and HSPi control group, the fluorescence intensity of GFP-TDP-43 NCs was rapidly recovered to approximately 72% and 70% of the pre-bleaching intensity in around 75 s (Figure 14H, 14K, Supplementary Figure S2A, S2B). In PR_{20} treated group, the fluorescence recovery was reduced to around 48% in 75s (Figure 14I, 14K). Of note, co-treatment of HSP70 inhibitor with PR_{20} (PR_{20}+HSPi) drastically decreased the fluorescence intensity of TDP-43 NCs to approximately 31% (Figure 14J, 14K), indicating that the fluidity of TDP-43 NCs is maintained by HSP70 chaperone upon transient poly-PR stress.

doi:10.6342/NTU202500138

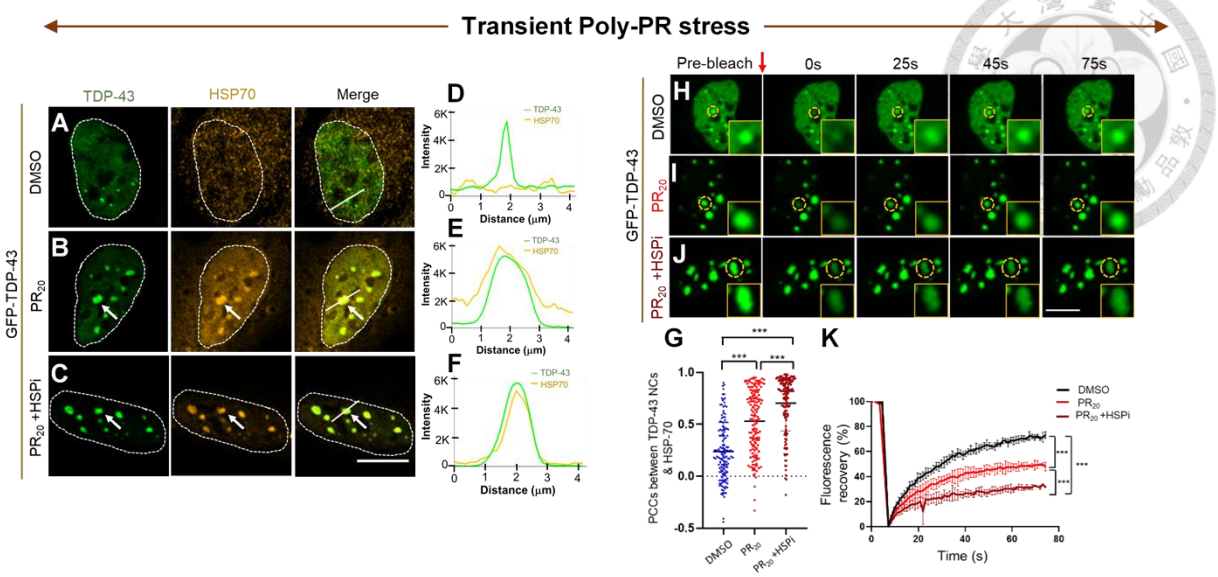

Figure 14. HSP70 maintains the fluidity of TDP-43 NCs under transient poly-PR stress. (A-C) Representative images of TDP-43 NCs following HSP70 inhibition. (D-F) Intensity profiles of TDP-43 NCs and HSP70 along the indicated lines in (A-C). The green line represents TDP-43 NCs, and the yellow line represents HSP70. (G) Pearson correlation coefficients (PCCs) showing the co-localization of TDP-43 NCs with HSP70. More than 140 independent cells were pooled and counted from three independent peptide treatments (N=3). (H-J) Representative FRAP images of TDP-43 NCs after PR_{20} and PR_{20}+HSPi treatments, with quantification of fluorescence recovery. A total of 36 NCs were bleached across three independent peptide treatments (N=3). (K) Quantification of fluorescence recovery after PR_{20} and PR_{20}+HSPi treatments. Error bars represent standard deviation; One-way ANOVA with Tukey's multiple comparison test was applied for (G), and Two-way ANOVA with Tukey's multiple comparison test was applied for (K), ***p<0.001. Scale bars, 10 μm (A-C, H-J).

3.11 Delocalization of HSP70 from TDP-43 NCs upon prolonged poly-PR stress induce phase transition of the condensates

Studies have shown that prolonged stress can induce phase transition and gelation of the TDP-43 NCs.[84,102,121] As poly-PR stress reduced the fluidity of TDP-43 NCs upon transient exposure (Figure 5E, 5F), we also monitored fluidity of the condensates upon

doi:10.6342/NTU202500138

prolonged exposure to poly-PR stress. First, we investigated whether HSP70 still colocalize with poly-PR induced TDP-43 NCs. Our immunostaining results showed that HSP70 did not colocalize with TDP-43 NCs (Figure 15B, 15E) similar to DMSO control (Figure 15A, 15D), suggesting prolonged poly-PR stress causes delocalization of HSP70 from TDP-43 NCs. While in PR_{20}+HSPi group HSP70 still colocalized within the condensates (Figure 15C, 15F), indicating HSP70 inhibition prevents its delocalization from TDP-43 NCs. Statistical analysis showed no increment in Pearson correlation coefficient between TDP-43 NCs and HSP70 upon prolonged poly-PR stress while PR_{20}+HSPi co-treatment showed significant increase (Figure 15G).

To confirm the aforementioned phenotype in live cells, we conducted time-lapse imaging. Upon PR_{20} treatment from 2 to 11 hours, colocalization and subsequent delocalization of HSP70 could be observed (Supplementary Figure S2G, S2H). In the control group, fewer TDP-43 NCs did not colocalize with HSP70 (Supplementary Figure S2E, S2F). Co-treatment of PR_{20}+HSPi showed enrichment of HSP70 within the induced TDP-43 NCs which persisted with time (Supplementary Figure S2I, S2J). These observations demonstrated that longer poly-PR stress led to delocalization of HSP70 from TDP-43 NCs.

To study the impact of HSP70 delocalization on TDP-43 NCs fluidity, we performed FRAP. In the DMSO and HSPi control group, the fluorescence intensity of GFP-TDP-43 NCs was rapidly recovered to approximately 75% and 70% of the pre-bleaching intensity in around 60 s (Figure 15H, 15K, Supplementary Figure S2C, S2D). In PR_{20} treated group, the fluorescence recovery was further reduced to around 36% in 60s (Figure 15I, 15K), which was even lower than transient poly-PR stress (Figure 5E, 5F, Figure 14I, 14K). Co-treatment

doi:10.6342/NTU202500138

of PR_{20}+HSPi had negligible effect on the fluorescence intensity of TDP-43 NCs with approximately 32% recovery (Figure 15J, 15K), suggesting HSP70 lost its fluidity maintenance function upon prolonged poly-PR stress. Altogether these findings indicate that delocalization of HSP70 from TDP-43 NCs upon prolonged poly-PR stress induced gelation of TDP-43 NCs.

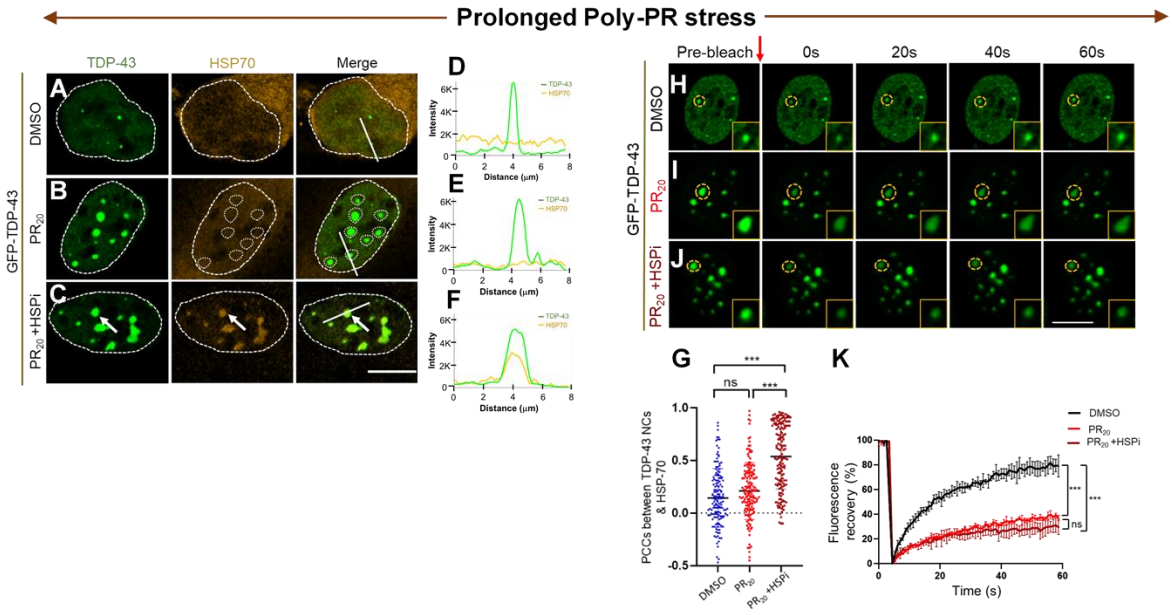

Figure 15. Delocalization of HSP70 upon prolonged poly-PR stress led to phase-transition of the TDP-43 NCs. (A-C) Representative images of TDP-43 NCs upon prolonged poly-PR stress. (D-F) The intensity profiles of TDP-43 NCs with HSP70 along the indicated lines in (A-C). Green line represents TDP-43 NCs, yellow line represents HSP70. (G) Pearson correlation coefficients (PCCs) reflect co-localization of TDP-43 NCs with HSP70. n>140 independent cells were pooled and counted from three independent peptide treatments (N=3). (H-J) Representative FRAP images of TDP-43 NCs upon PR_{20} and PR_{20}+HSPi treatment were quantified for fluorescence recovery. n= 36 NCs were bleached from three independent peptide treatments (N=3). (K) Quantification of fluorescence recovery upon prolonged PR_{20} and PR_{20}+HSPi treatment. Error bar corresponds to standard deviation; One-way ANOVA with Tukey's multiple comparison test was used to analyze (G), Two-way ANOVA with Tukey's multiple comparison test was used to analyze (K), ***p<0.001, ns= non-significant. Scale bars, 10 μm (A-C, H-J).

doi:10.6342/NTU202500138

3.12 *NEAT1* participate in TDP-43 NCs formation even upon prolonged poly-PR stress but no longer involved in HSP70 recruitment

Prolonged poly-PR stress resulted in delocalization of HSP70 from TDP-43 NCs and loss of its protective role. Under transient poly-PR stress, *NEAT1* RNA promoted TDP-43 NCs formation and HSP70 recruitment. To check the role of *NEAT1* upon prolonged poly-PR stress, we knockdown *NEAT1* by and conducted immunostaining followed by RNA-FISH to examine its functionality. Our results showed that in siCtrl group with longer PR_{20} dipeptide (+PR_{20}) treatment, *NEAT1* still colocalized with induced TDP-43 NCs (Figure 16B). compared to untreated group (-PR_{20}) (Figure 16A). Knocking down of *NEAT1* (si*NEAT1*) reduced TDP-43 NCs number in both +PR_{20} and -PR_{20} group (Figure 16C, 16D). The statistical analysis depicts reduction in TDP-43 NCs count upon *NEAT1* knockdown (Figure 16E), suggesting *NEAT1* maintains its function of promoting TDP-43 nuclear condensation upon prolonged poly-PR stress.

We also examined HSP70 localization with respect to TDP-43 NCs upon *NEAT1* knockdown. Similar to aforementioned results (Figure 15B, 15E), no enrichment of HSP70 could be observed in TDP-43 NCs (Figure 16B) and the Pearson correlation coefficient did not increase with or without PR_{20} treatment (Figure 16G). These observations suggests that the delocalization of HSP70 from TDP-43 NCs was independent of *NEAT1*. Similar to the previous literature,[68] we also observed that prolonged poly-PR stress upregulated *NEAT1* (Figure 16F) which was not observed under transient poly-PR stress (Supplementary Figure 3).

doi:10.6342/NTU202500138

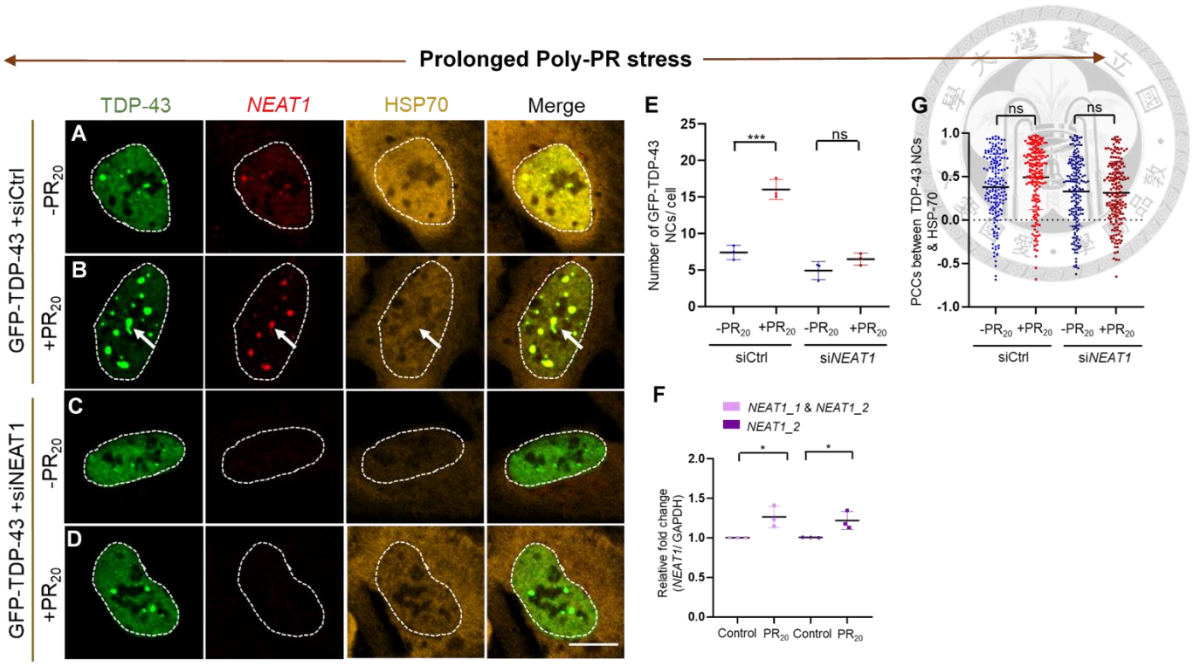

Figure 16. *NEAT1* promotes TDP-43 nuclear condensation but not HSP70 recruitment upon prolonged poly-PR stress. (A-D) Representative images of TDP-43 NCs following *NEAT1* knockdown (si *NEAT1*) with or without 5 μM PR_{20} dipeptide treatment for 12 hours, probed for *NEAT1* and immunostained for HSP70 using immunostaining and RNA-FISH. (E) Quantification of the number of GFP-TDP-43 NCs after prolonged poly-PR stress. More than 160 independent cells were pooled and counted from three independent peptide treatments (N=3). (F) qPCR analysis demonstrated upregulation of *NEAT1* isoforms following 5 μM PR_{20} treatment for 12 hours. Quantitative real-time PCR analysis was performed to monitor the relative fold change of *NEAT1* from three independent peptide treatments (N=3). (G) Pearson correlation coefficients (PCCs) showing the co-localization of GFP-TDP-43 NCs with HSP70 following *NEAT1* knockdown and prolonged poly-PR treatment. More than 160 independent cells were pooled and counted from three independent peptide treatments (N=3). Error bars represent standard deviation; One-way ANOVA with Tukey's multiple comparison test was used for (E), (F), and (G). *p<0.05, ***p<0.001, ns = non-significant. Scale bars, 10 μm (A-D).

doi:10.6342/NTU202500138

3.13 Localization of *NEAT1* and HSP70 in TDP-43 NCs is consistent in neuronal cell-line under poly-PR stress duration

Our observations in U2OS cell line showed that although *NEAT1* colocalized with TDP-43 NCs throughout poly-PR stress duration, HSP70 localization changed with poly-PR stress duration. To observe these phenotypes in a more disease-relevant cell type, we created eGFP-TDP-43 expressing N2a neuronal cell line (Figure 17A) and checked for the expression of overexpressed eGFP-TDP-43 using western blot. The overexpression of eGFP-TDP-43 was not too high (~0.7) compared to the endogenously expressed TDP-43 (Figure 17B, 17C). As expected, upon transient poly-PR stress, TDP-43 NCs number increased and colocalized with both *NEAT1* and HSP70 (Figure 17E, 17G, 17I, 17K, 17T) compared to control (Figure 17D, 17F, 17H, 17J, 17T). Upon prolonged poly-PR stress, the increase in TDP-43 NCs number persisted (Figure 17T) and HSP70 delocalized from these condensates (Figure 17M, 17O). The control also showed no HSP70 enrichment within TDP-43 NCs (Figure 17L, 17N). In addition, *NEAT1* colocalization was still observed within the TDP-43 NCs (Figure 17Q, 17S) compared to control (Figure 17P, 17R). These findings suggests that TDP-43 NCs formation and distribution of the aforementioned cellular components upon poly-PR stress duration is consistent in neuronal cell type.

doi:10.6342/NTU202500138

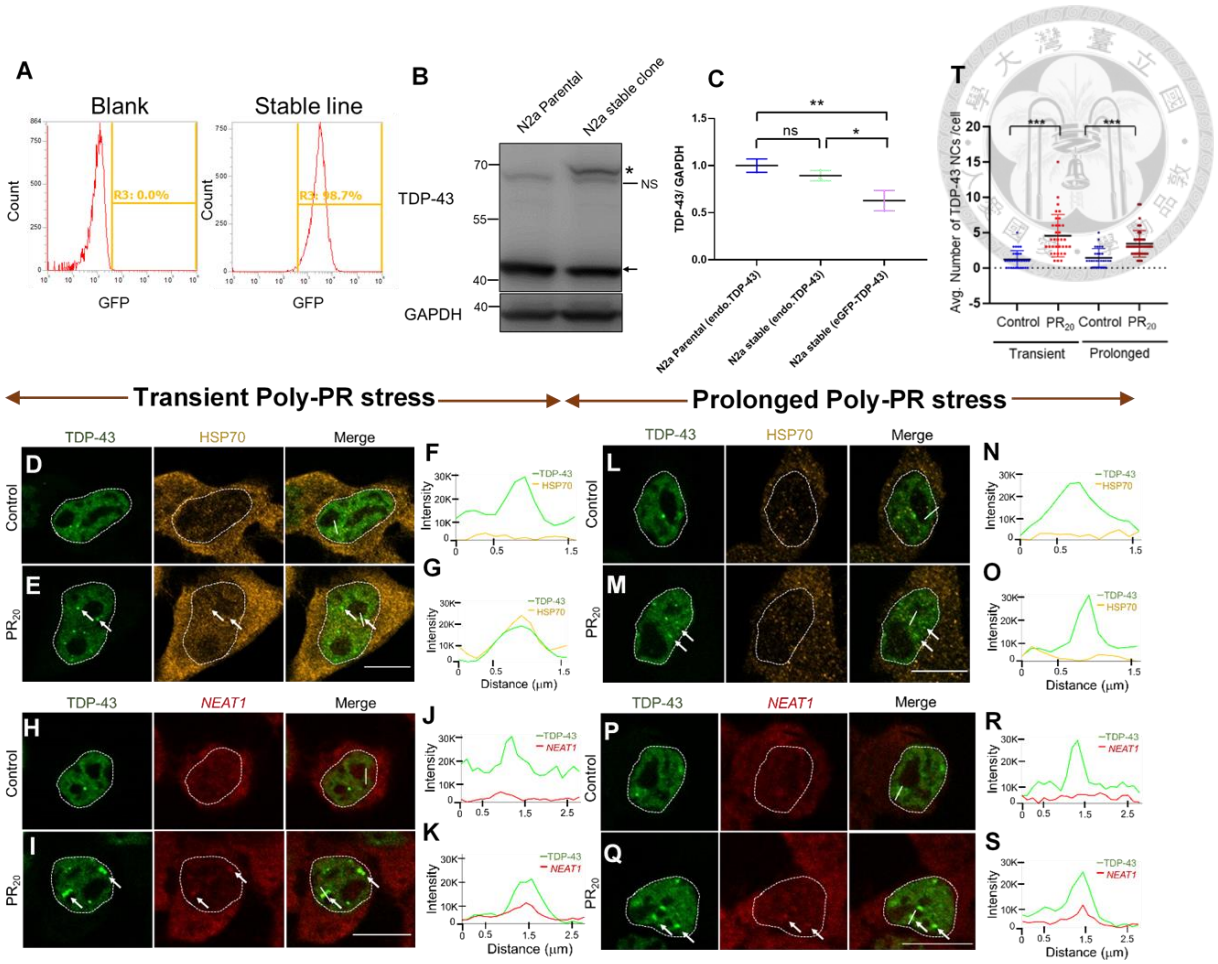

Figure 17. Transient and prolonged poly-PR stress causes colocalization and subsequent delocalization of HSP70 but not *NEAT1* from TDP-43 NCs. (A) Flow cytometry analysis of eGFP-TDP-43 expressing N2a stable cell line compared to blank (untransfected cells). The red peak within the eGFP expression gate indicates that more than 98% of the cells in this clone stably express eGFP-TDP-43. (B, C, K, L) Representative images of TDP-43 NCs following 5 μM PR_{20} treatment for 12 hours (transient) and 24 hours (prolonged) in N2a cells, immunostained with HSP70. White arrows indicate co-localization of TDP-43 NCs with HSP70 during transient poly-PR stress, while orange arrows indicate subsequent delocalization of HSP70 from NCs during prolonged poly-PR stress. Dashed line represents the nucleus. (F, G, O, P) Representative images of TDP-43 NCs following 5 μM PR20 treatment for 12 hours (transient) and 24 hours (prolonged) in U2OS cells, probed for NEAT1. White arrows indicate co-localization of TDP-43 NCs with *NEAT1* during both transient and prolonged poly-PR stress. (D, E, H, I, M, N, Q, R) Intensity profiles of GFP-TDP-43 NCs with either HSP70 or *NEAT1* along the line indicated in (B, C, F, G, K, L, O, P). The green line represents GFP-TDP-43 NCs, the yellow line represents HSP70, and the red line represents *NEAT1*. (J) Quantification of the number of TDP-43 NCs per cell. More than 30 independent cells were analyzed from one peptide treatment. Error bars represent

doi:10.6342/NTU202500138

standard deviation; One-way ANOVA with Tukey's multiple comparisons test was used for (J). ***p<0.001. Scale bars, 10 μm (B, C, F, G, K, L, O, P).

3.14 Prolonged poly-PR stress induced gel-like NCs are rich in TDP-43 oligomers

Previous literature has shown that arsenite stress induced gel-like TDP-43 NCs contained a lot of oligomers.[121] In line with these findings, we also examined the oligomerization status of TDP-43 protein within the poly-PR induced gel-like TDP-43 NCs. To achieve this, we applied fluorescence lifetime imaging microscopy (FLIM) Förster resonance energy transfer (FRET), A11 immunostaining and filter trap assay. FLIM-FRET is a microscopy technique which measure energy transfer through the dipole–dipole coupling of a fluorescent donor and acceptor[122] for monitoring oligomeric species of proteins.[123,124] For the donor and acceptor, we co-expressed eGFP-TDP-43 (donor) and mCherry-TDP-43 (acceptor) in U2OS cell. (Supplementary Figure S4A-D and S4A'-D'). By utilizing time-domain lifetime fitting analysis (frame model),[103] we measured the FRET efficiency maps (Figure 18A'-18D') from the FLIM-FRET images (Figure 18A-18D) upon both transient and prolonged poly-PR stress. The data showed that transient poly-PR stress did not increase the FRET efficiency (E_{FRET}) of poly-PR treated group (Figures 18B, 18B' and 18E) compared to control (Figures 18A, 18A' and 18E), with E_{FRET} approximately 18% in both the groups. By contrast, the E_{FRET} upon prolonged poly-PR stress increased to 24% (Figures 18D, 18D' and 18E) compared to 18% in control (Figures 18C, 18C' and 18E). The increase in FRET efficiency indicates that prolonged poly-PR stress promotes high-ordered conformation of TDP-43 within the condensates. Similar conclusion was also confirmed by applying

doi:10.6342/NTU202500138

oligomer-specific A11 antibody which recognize TDP-43 oligomers with high-order conformation.[123,125,126] Upon transient poly-PR stress (18G, 18I, 18N), no enrichment of A11 intensity was observed within the condensates compared to control (18F, 18H, 18N). However, under prolonged poly-PR treatment, cells showed enrichment of A11 signal within the condensates (18K, 18M, 18N) compared to control (18J, 18L, 18N). In addition, we also performed filter-trap assay to ensure oligomerization of TDP-43 upon poly-PR stress.[123,127] The intensity of A11 on the blot upon prolonged poly-PR stress was increased compared to control and transient poly-PR stress group (Figure 18O, 18P). Altogether, these findings confirmed the oligomerization of TDP-43 upon prolonged poly-PR stress.

doi:10.6342/NTU202500138

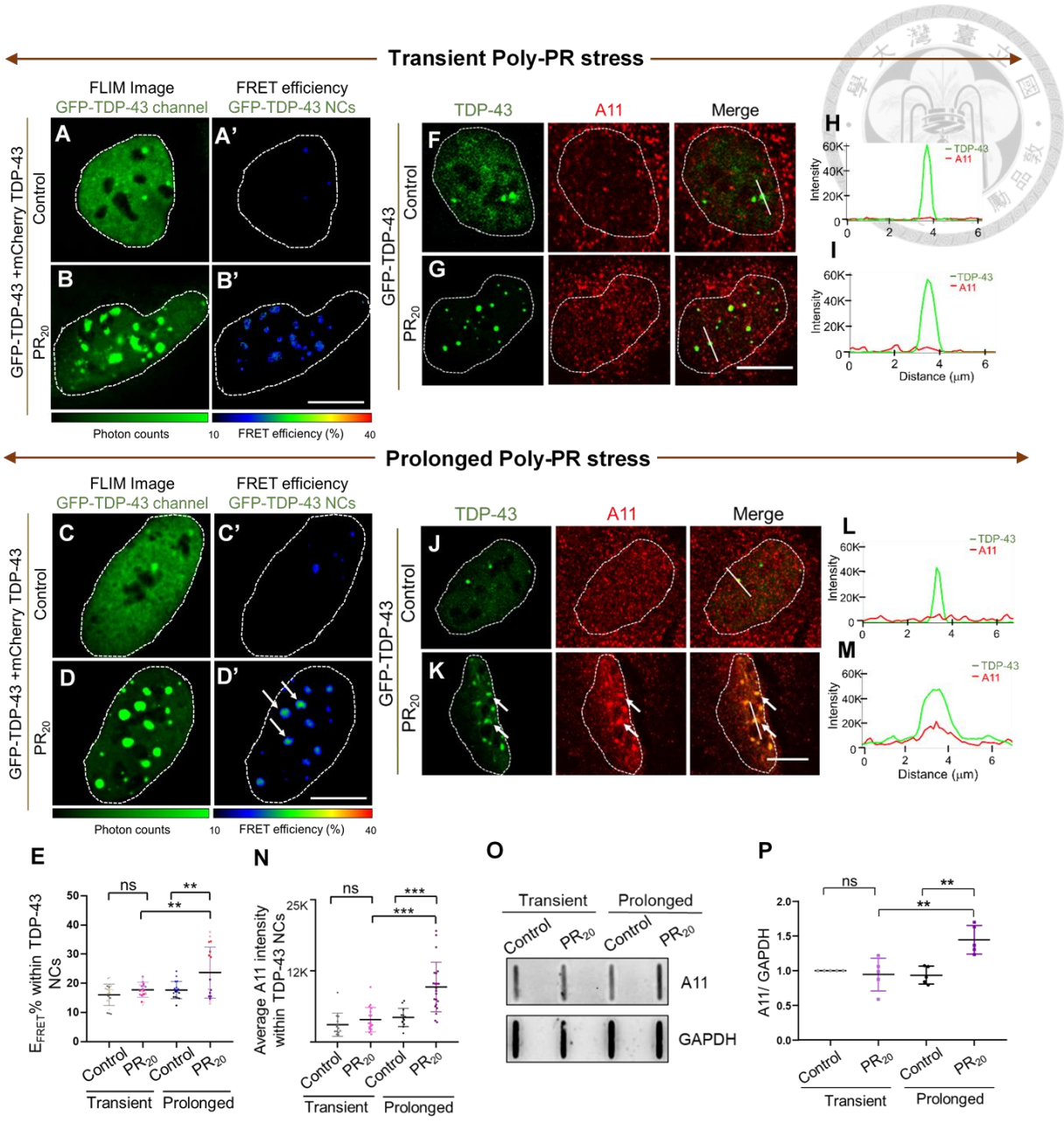

Figure 18. Prolonged poly-PR stress promotes oligomerization of TDP-43 within NCs. (A-D) Representative FastFLIM images of GFP-TDP-43 donor co-transfected with eGFP-TDP-43 and mCherry-TDP-43 plasmids in U2OS cells under 4 hours (transient) and 12 hours (prolonged) of poly-PR stress. The color palette (shown at the bottom) corresponds to the brightness of GFP-TDP-43. Dashed line marks the nucleus. (A'-D') Representative color-coded E_{FRET} images ("highlighted-pixel" fitting model) from eGFP-TDP-43 and mCherry-TDP-43 co-expressed cells. The color palette (shown at the bottom) indicates the E_{FRET} levels of TDP-43 species (monomers + oligomers) within the TDP-43 NCs. Arrows point to areas of increased E_{FRET} under prolonged poly-PR stress. Dashed line represents nucleus. (E)

doi:10.6342/NTU202500138

Average E_{FRET} values for panels A'–D'. More than 15 cells were arbitrarily selected, and the region average lifetime was calculated on a pixel-by-pixel basis. Data were pooled and analyzed from three independent peptide treatments (N=3). (F, G, J, K) Representative images of GFP-TDP-43 NCs under transient and prolonged poly-PR stress, immunostained with oligomer-specific A11 antibody. Arrows indicate enhanced co-localization of TDP-43 NCs with A11 under prolonged poly-PR stress. Dashed line marks the nucleus. (H, I, L, M) Intensity profiles of GFP-TDP-43 NCs with A11 along the lines indicated in (F, G, J, K). The green line represents GFP-TDP-43 NCs, and the red line represents A11 signal. (N) Quantification of A11 intensities within TDP-43 NCs. More than 15 independent cells were analyzed from a single peptide treatment. (O) Filter trap assay of eGFP-TDP-43 expressing U2OS cells under transient and prolonged poly-PR stress. The cell lysate was loaded onto a nitrocellulose (NC) membrane and probed with A11 (upper) and GAPDH (lower) antibodies (loading control). A red rectangle highlights the increased A11 signal under prolonged poly-PR stress. (P) Quantification of the blot in panel (O). Data were analyzed from five independent peptide treatments (N=5). Error bars represent standard deviation; One-way ANOVA with Tukey's multiple comparison test was used for (E), (N), and (P). **$p<0.01$, ***$p<0.001$, ns = non-significant. Scale bars, 10 μm (A-D, A'-D', F, G, J, K).

3.15 Prolonged poly-PR stress induces TDP-43 proteinopathy and cell death

Gel-like oligomeric TDP-43 NCs are sometimes accompanied with phosphorylated and ubiquitinated TDP-43 aggregates under several stresses.[102,128] Therefore, we also examined whether our poly-PR induced gel-like TDP-43 NCs are positive for the aforementioned markers. Our immunostaining data showed that prolonged poly-PR stress induced TDP-43 NCs are phosphorylated but not ubiquitinated (Figures 19B) compared to control (Figures 19A), suggesting aggregation of TDP-43. To confirm phosphorylation, we also performed western blot analysis. The blot showed increased intensity of pTDP-43 upon prolonged poly-PR stress (Figures 19C, 19D), confirming longer poly-PR stress indeed causes TDP-43 aggregation. In addition, we also monitored C-terminal fragments of TDP-

doi:10.6342/NTU202500138

43 upon poly-PR stress, which is an important hallmark of TDP-43 proteinopathy.[79] Our western blot data showed that prolonged poly-PR stress increased the intensity of 25KDa C-terminal TDP-43 fragments compared to control (arrow indicated in Figure 19E). The statistical analysis showed significant increase in the intensity of C-terminal TDP-43 fragments upon poly-PR stress (Figure 19F).

Aberrant aggregation of TDP-43 NCs may subsequently lead to cytosolic TDP-43 proteinopathy.[129] To investigate the impact of prolonged poly-PR stress on TDP-43 mislocalization, we monitored cytosolic TDP-43. Our results showed that in the control group around 14% TDP-43 mislocalization was observed (Figures 19G, 19I) while prolonged poly-PR stress further increased the mislocalization to 29% (Figures 19H, 19I). To investigate the toxic effect of prolonged poly-PR stress induced TDP-43 proteinopathy, we conducted LDH toxicity assay. In the control group, the cytotoxicity was around 3.3% (Figure 19J). Upon prolonged treatment to poly-PR dipeptide the cell death increased to around 7.7% (Figure 19J). Altogether, these findings indicate that along with gelation and oligomerization of TDP-43 NCs, prolonged poly-PR stress induced TDP-43 proteinopathy may jointly involve in poly-PR induced cytotoxicity.

doi:10.6342/NTU202500138

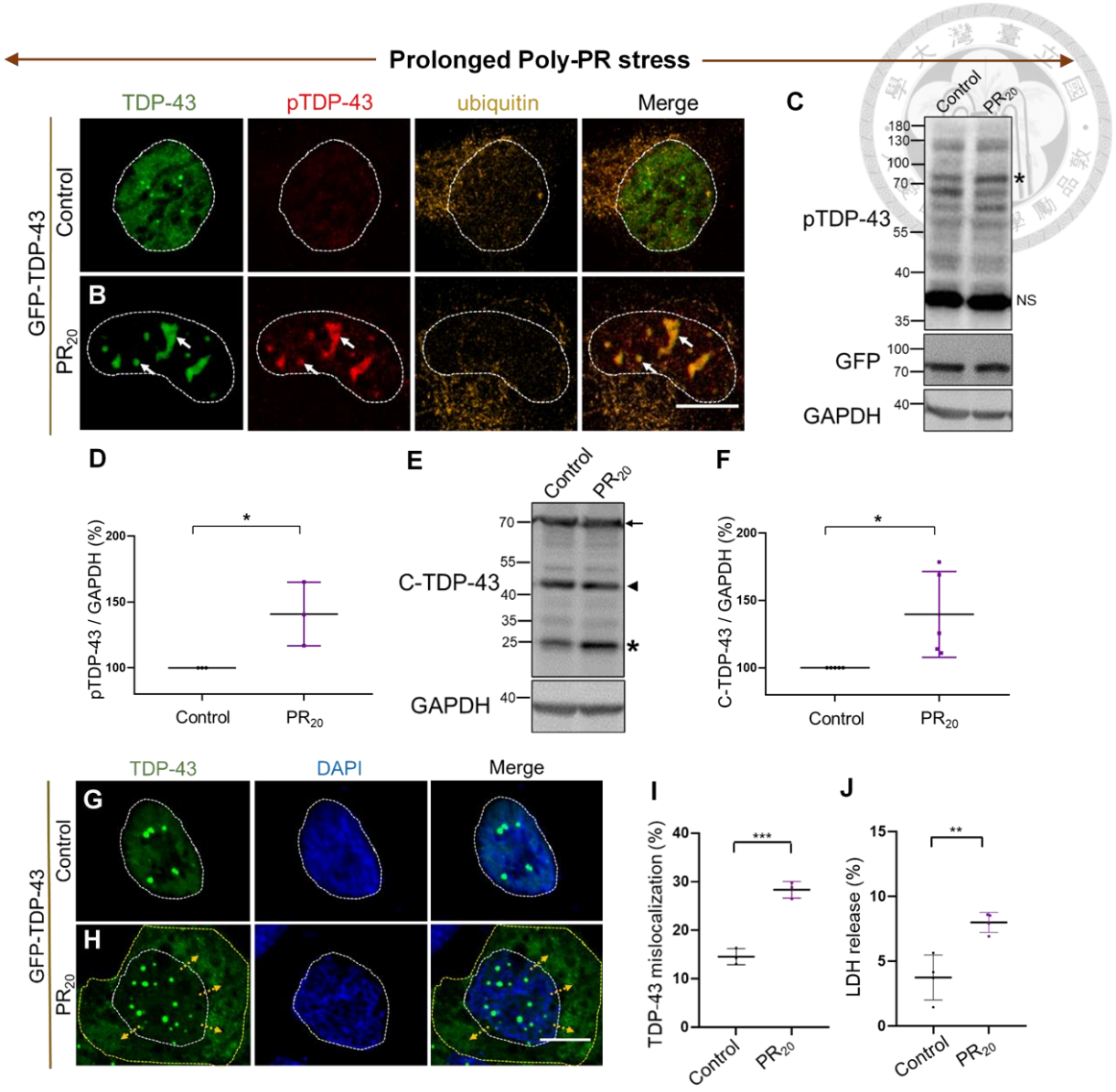

Figure 19. Prolonged poly-PR stress induced TDP-43 proteinopathy and cell death. (A-B) Representative images of GFP-TDP-43 NCs immunostained with pTDP-43 and ubiquitin antibodies after prolonged poly-PR stress. Arrows highlight the co-localization of TDP-43 NCs with phospho-TDP-43 in the PR20-treated group. (C) Western blot analysis of phospho-TDP-43 showing an enhanced p-TDP-43 signal after prolonged poly-PR stress compared to control. (D) Quantification of pTDP-43 signal after poly-PR peptide treatment in three independent repeats (N=3). (E-F) Representative images showing mislocalized TDP-43 after prolonged poly-PR stress. Arrows indicate mislocalization of TDP-43 to the cytosol in the PR20-treated group. (G) Quantification of mislocalized TDP-43 following poly-PR peptide

doi:10.6342/NTU202500138

treatment in three independent repeats (N=3). (H) Western blot analysis of C-terminal TDP-43 fragments, showing an enhanced 25 kDa C-terminal TDP-43 fragment after prolonged poly-PR stress compared to control (indicated by asterisk). The 43 kDa band represents endogenous TDP-43 (indicated by the arrowhead), while the 70 kDa band represents eGFP-tagged TDP-43 (indicated by the arrow). (J) Cytotoxicity analysis after prolonged poly-PR treatment in three independent repeats (N=3). Error bars represent standard deviation; unpaired t-test was used for analysis in (D), (I), (G), (J). *$p<0.05$, **$p<0.01$, ***$p<0.001$. Scale bars, 10 μm (A, B, E, F).

doi:10.6342/NTU202500138

4 Discussion

Nuclear condensation of TDP-43 has been recently studied under various stresses and found to be associated with ALS.[57,84,130] *C9ORF72* gene encoded arginine-rich dipeptides, Poly-PR and Poly-GR, induce phase-separation of TDP-43 and perturbs the dynamics of various membraneless organelles.[42,64,131,132] Yet, the effect of these dipeptides on nuclear condensation of TDP-43 is not well studied. In this study, we specifically investigated the effect of arginine-rich dipeptides on TDP-43 nuclear condensation. We found that poly-PR induce the nuclear condensation of TDP-43, but this appears to be an indirect effect since the poly-PR dipeptide present in the nucleolus did not colocalize with TDP-43 NCs. As the interaction is found to be an indirect event, we had two hypothesis (1) nucleolar occupying poly-PR may generate nucleolar stress that caused TDP-43 NCs induction. (2) Change in the RNA levels by poly-PR may result in alteration of RNA-bound to TDP-43 causing the latter to undergo LLPS. Our results indicated that poly-PR dipeptide did not cause any proteasomal stress, therefore we suspect that the transcriptome change upon poly-PR stress could lead to TDP-43 LLPS in the nucleus and further transcriptome analysis may provide new insights into poly-PR driven TDP-43 nuclear LLPS. Many membranelles organelles (like the nucleolus and paraspeckles) share their proteomes and interact with each other under stress.[133] The changes in nucleolar proteome upon poly-PR stress may led to nuclear condensation of TDP-43. Therefore, the alteration of both protein and in RNA homeostasis upon poly-PR stress may result in TDP-43 nuclear condensation.[88] Overall, we propose that changes in nucleolar composition by poly-PR dipeptide[42,66] led to nuclear LLPS of TDP-43.

doi:10.6342/NTU202500138

TDP-43 is a DNA/RNA-binding protein that preferentially interacts with long UG-rich RNA sequences.[134] The long form of *NEAT1* lncRNA (*NEAT1_2*) contains three regions rich in UGUG sequence which complements binding target of TDP-43 protein.[98] In addition, *in-vitro* studies have shown that *NEAT1* is an important lncRNA that participate in TDP-43 droplet formation.[84] The formation of *NEAT1*-positive TDP-43 nuclear bodies are regarded as protection mechanism of the cell against oxidative stress.[84,93] In addition, such organelles may also function as global sensors in response to various stressors.[135] In our study, we reported that both transient and prolonged poly-PR stress induce the formation of TDP-43 NCs in a *NEAT1*-dependent manner, which could be a cellular mechanism for coping with poly-PR stress. Upon transient poly-PR stress, upregulation of *NEAT1* was not observed. However, prolonged poly-PR stress demonstrated *NEAT1* upregulation, which could be linked to cytotoxicity and TDP-43 proteinopathy.[68,97,98] The increased levels of *NEAT1* may lead to the increased self-interaction of TDP-43 and *NEAT1* within the condensates[136], resulting in conformation change of TDP-43[137] and its oligomerization within the condensates. Therefore, we hypothesize that the formation of TDP-43 NCs upon poly-PR stress was initially a protective mechanism which turned around upon *NEAT1*-upregulation along with perturbation of HSP70 localization.

Studies have highlighted the important role of chaperones in preserving the liquid-like properties of TDP-43 NCs and preventing their inappropriate phase transitions.[57,85,102] In this study, we demonstrated that HSP70 sustains the fluidity of TDP-43 NCs upon transient poly-PR stress. Of note, prolonged poly-PR stress results in delocalization of HSP70 from the condensates leading to reduced fluidity, which is another turn-around event for loss of

doi:10.6342/NTU202500138

TDP-43 NCs protective ability. Additionally, the gel-like TDP-43 NCs were found to be phosphorylated, hallmark of TDP-43 aggregation. These findings align with the behavior of TDP-43 phase separation and phosphorylation observed under other stress conditions.[102,128] The gelation of TDP-43 NCs was accompanied with oligomerization of TDP-43 within these condensates, suggesting the correlation between phase transition of droplets and aggregation of the protein within the droplets. Our study also reported that prolonged Poly-PR stress caused C-terminal truncation of TDP-43, and its cytoplasmic mislocalization, hallmark of ALS.[79] This hints the *C9ORF72* encoded dipeptides may predispose TDP-43 towards its aggregation in nucleus and TDP-43 proteinopathy. Altogether through our study, we propose that the aberrant TDP-43 LLPS and its proteinopathy parallelly contributes to poly-PR-mediated toxicity.

This study simultaneously examined the roles of *NEAT1* RNA and HSP70 chaperone in poly-PR-induced TDP-43 nuclear condensation and the subsequent phase transition. While *NEAT1*-mediated TDP-43 NCs are thought to be protective, the delocalization of HSP70 from the condensates during prolonged poly-PR stress altered their protective role. Given that the accumulation of these dipeptides is believed to be an early event in ALS progression, they may predispose TDP-43 to subsequent proteinopathy.[138] Supporting this notion, our study revealed that *C9ORF72*-ALS associated poly-PR toxicity is contributed by both aberrant TDP-43 nuclear LLPS and its subsequent proteinopathy.

doi:10.6342/NTU202500138

5 Summary

Our study demonstrated that TDP-43 nuclear condensation and its aberrant phase transition plays role in *C9ORF72* poly-PR mediated-toxicity (Figure 20). Upon transient poly-PR stress, TDP-43 condenses in the nucleus with participation of *NEAT1* and HSP70. While *NEAT1* mediates the formation of the condensates, HSP70 maintains the fluidity of these condensates. The enhanced formation of TDP-43 NCs is regarded as a protective mechanism of the cells against poly-PR stress. However, upon prolonged poly-PR stress, delocalization of HSP70 from TDP-43 NCs promotes the gelation of these condensates. Moreover, the gelation is also accompanied with oligomerization and phosphorylation of TDP-43 within these condensates. Prolonged poly-PR stress also led to nuclear-to-cytosolic mislocalization and fragmentation of TDP-43, resulting in ALS-associated TDP-43 proteinopathy. Altogether, the aberrant LLPS of TDP-43 and its proteinopathy contributes to poly-PR associated toxicity mechanism.

doi:10.6342/NTU202500138

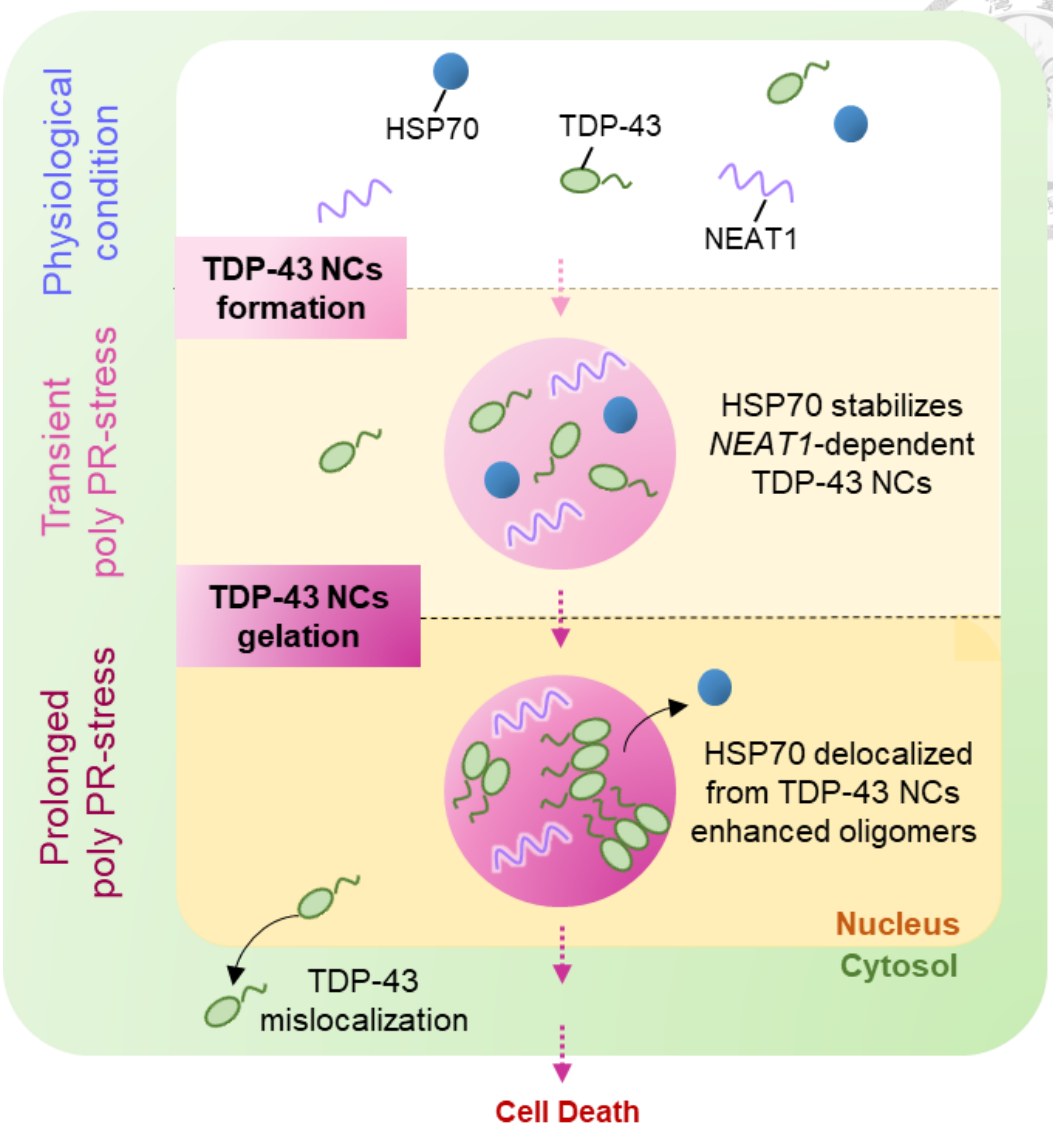

Figure 20. Schematic illustration of poly-PR induced TDP-43 nuclear condensation. Transient poly-PR stress induces TDP-43 nuclear condensation facilitated by *NEAT1* lncRNA and HSP70 chaperone. Upon prolonged poly-PR stress, HSP70 delocalize from the condensates triggering oligomerization of TDP-43 within the condensates. Prolonged Poly-PR induced TDP-43 proteinopathy along with its oligomerization promote cytotoxicity.

doi:10.6342/NTU202500138

6 Supplementary Figures

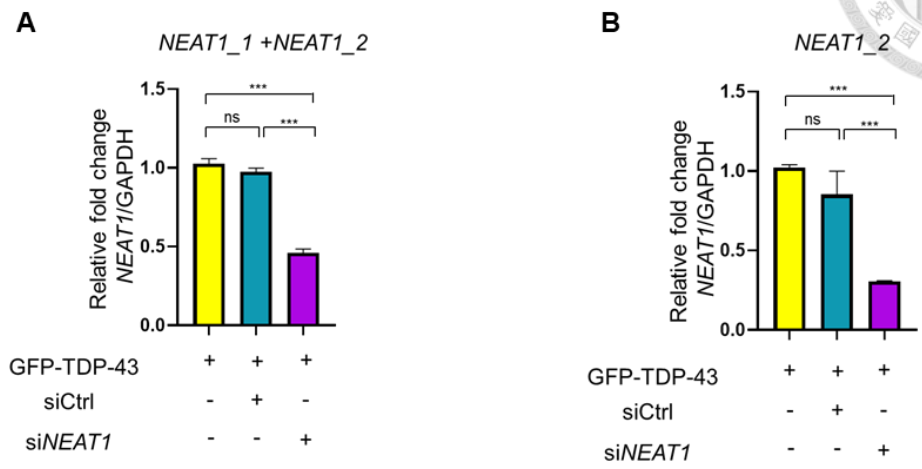

Supplementary Figure 1 (A, B) qPCR analysis to quantify the relative fold-change following depletion of both *NEAT1* isoforms (*NEAT1_1* & *NEAT1_2*; Total, *NEAT1_2*; long-form). The experiment was conducted in three independent repeats (N=3). Error bars represent standard deviation; One-way ANOVA with Tukey's multiple comparisons test was used in (A) and (B). ***p<0.001, ns = non-significant.

doi:10.6342/NTU202500138

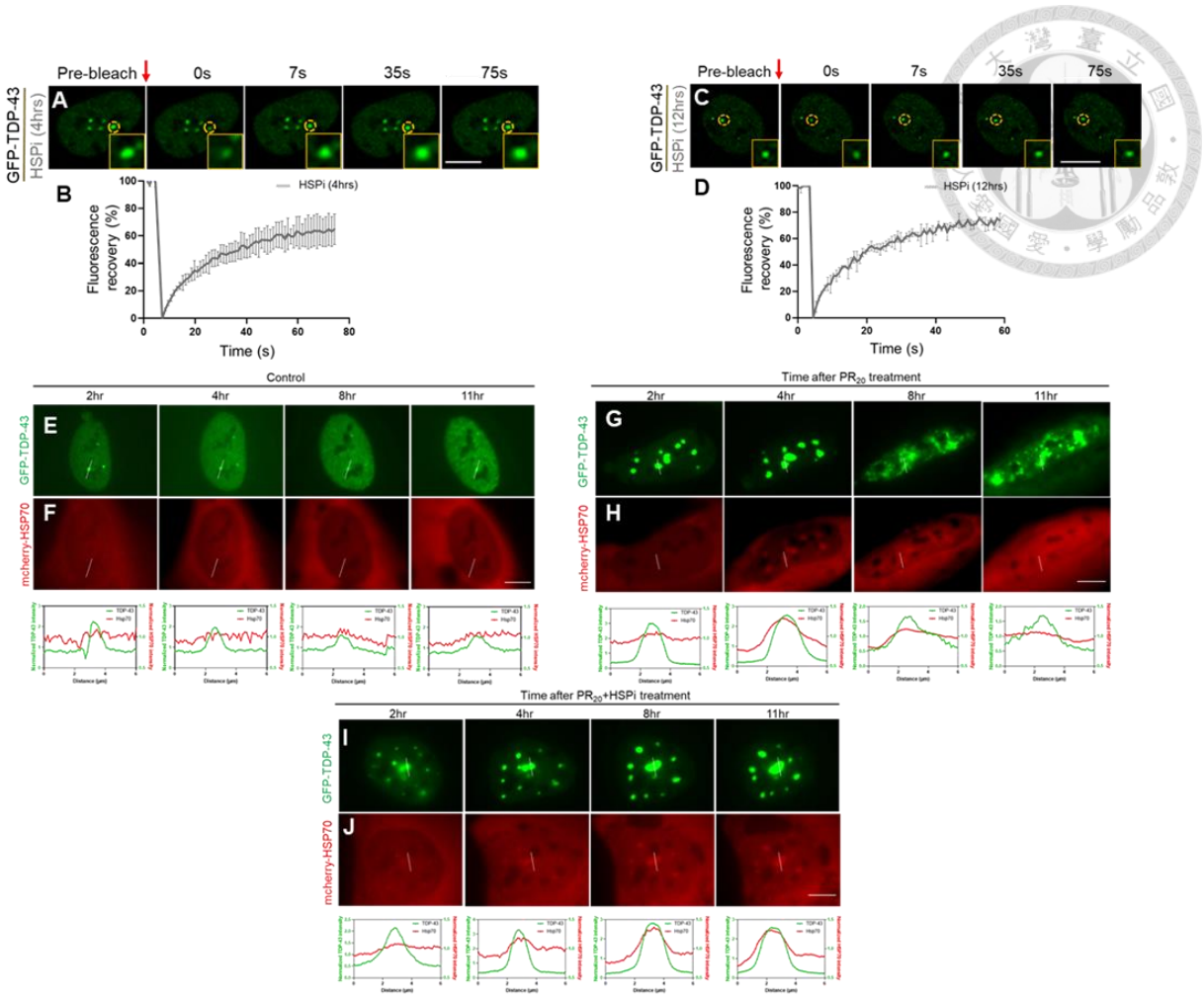

Supplementary Figure 2. Inhibition of HSP70 alone did not affect the fluidity of TDP-43 NCs, both under transient and prolonged exposure, nor did it impact the delocalization of HSP70 upon poly-PR stress over time. (A, C) FRAP images of GFP-TDP-43 NCs in cells after treatment with 50 μM of HSP70 inhibitor (HSPi) for 4 hours (transient) and 12 hours (prolonged), respectively. (B, D) Fluorescence recovery analysis of GFP-TDP-43 NCs following HSPi treatment. n = 36 NCs were bleached and analyzed from three independent HSPi treatments (N = 3). (E-J) Time-lapse imaging to monitor HSP70 delocalization over 2 to 11 hours in control, PR_{20}, and PR_{20} + HSPi co-treatment groups. Scale bars, 10 μm (A, C, E-J).

doi:10.6342/NTU202500138

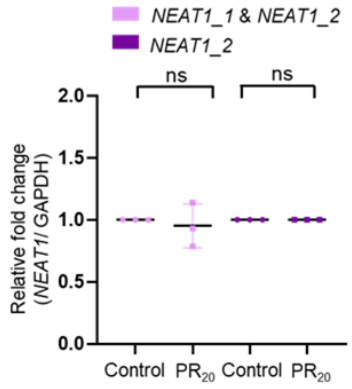

Supplementary Figure 3. qPCR analysis reveals no upregulation of *NEAT1* isoforms after 5 μM of PR_{20} treatment for 4 hours. Quantitative real-time PCR was conducted to assess the relative fold change of *NEAT1*, based on three independent peptide treatments (N=3).

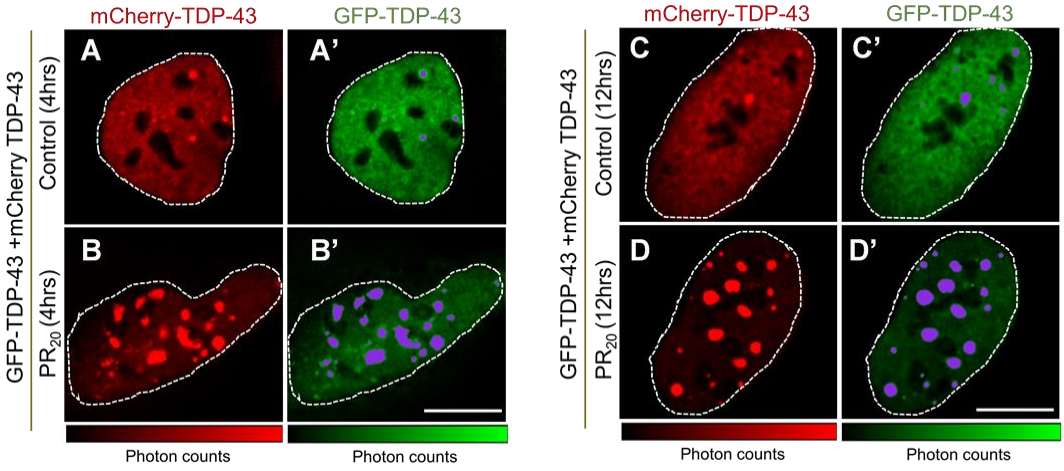

Supplementary Figure 4. (A-D) Representative FastFLIM images of mCherry-TDP-43 acceptor in GFP-TDP-43 and mCherry-TDP-43 co-expressed U2OS cells following 4 hours (transient) and 12 hours (prolonged) of PR_{20} treatment. The color palette (shown at the bottom) represents the brightness of mCherry-TDP-43. (A'-D') The highlighted region (purple) from figures S4A-5D, used for the "frame" fitting analysis.

doi:10.6342/NTU202500138

7 Supplementary Tables

Table S1. Primers used for plasmid construction, related to STAR Methods.

Name	Sequence
FUS-eGFP-F:	5’–CTTCCTCGAGATGGCCTCAAACGATTATACC –3’
FUS-eGFP-R:	5’–CAACGGATCCTATACGGCCTCTCCCTGCGATC – 3’
eGFP-NLS_F:	5’–AAAAAAGAAGAGAAAGGTACGAGCTCAAGCTTCGAATTCTGC –3’
eGFP-NLS_R:	5’– TTTCTCTTCTTTTTTGGAGATCTGAGTCCGGACTTGTACAGC –3’
mCherry-TDP-43-F:	5’–GCATACCGGTATGGTGAGCAAGGGCGAGG –3’
mCherry-TDP-43-R	5’–CAGTGAGCTCCTTGTACAGCTCGTCCATGC –3’
mCherry-HSPA1A Fragment1_ F:	5’–TCAGATCTCGAGCTCAAGCTTATGGCCAAAGCCGCGGCG –3’
mCherry-HSPA1A Fragment1_ R:	5’–CGTCGCGCAGAGCCTTCTCCACGGGCTCC –3’
mCherry-HSPA1A Fragment2_ F:	5’–GGAGAAGGCTCTGCGCGACGCCAAGCTGG –3’’
mCherry-HSPA1A Fragment2_ R:	5’–TTATCTAGATCCGGTGGATCCCTAATCTACCTCCTCAATGGTGGGG –3’

doi:10.6342/NTU202500138

Table S2. Primers used for qPCR, related to STAR Methods.

Name	**Sequence**
Total *NEAT1_1* + *NEAT1_2_* F:	5’ – CAGGAGCTGGAAGTCTTAGAAA – 3’
Total *NEAT1_1* + *NEAT1_2_* R:	5’ – CCAGAAGAGCCCATCTAATCTC –3’
Long form *NEAT1_2_* F:	5’ – TTCTGCTTTCTGCCCATGTA – 3’
Long form *NEAT1_2_* R:	5’ – CAACCACAACAGGTGGATTATTT –3’
GAPDH_F:	5’ – AGCCTCAAGATCATCAGCAAT –3’
GAPDH_R:	5’ – GTCATGAGTCCTTCCACGATAC –3’

doi:10.6342/NTU202500138

8 References

1. Keon, M., Musrie, B., Dinger, M., Brennan, S.E., Santos, J., and Saksena, N.K. (2021). Destination Amyotrophic Lateral Sclerosis. Front Neurol *12*, 596006. 10.3389/fneur.2021.596006.
2. Masrori, P., and Van Damme, P. (2020). Amyotrophic lateral sclerosis: a clinical review. Eur J Neurol *27*, 1918-1929. 10.1111/ene.14393.
3. Brown, R.H., Jr., and Al-Chalabi, A. (2017). Amyotrophic Lateral Sclerosis. N Engl J Med *377*, 1602. 10.1056/NEJMc1710379.
4. Longinetti, E., and Fang, F. (2019). Epidemiology of amyotrophic lateral sclerosis: an update of recent literature. Curr Opin Neurol *32*, 771-776. 10.1097/WCO.0000000000000730.
5. Renton, A.E., Chio, A., and Traynor, B.J. (2014). State of play in amyotrophic lateral sclerosis genetics. Nat Neurosci *17*, 17-23. 10.1038/nn.3584.
6. Brown, R.H., and Al-Chalabi, A. (2017). Amyotrophic Lateral Sclerosis. N Engl J Med *377*, 162-172. 10.1056/NEJMra1603471.
7. Rosen, D.R., Siddique, T., Patterson, D., Figlewicz, D.A., Sapp, P., Hentati, A., Donaldson, D., Goto, J., O'Regan, J.P., Deng, H.X., and et al. (1993). Mutations in Cu/Zn superoxide dismutase gene are associated with familial amyotrophic lateral sclerosis. Nature *362*, 59-62. 10.1038/362059a0.
8. Ticozzi, N., Silani, V., LeClerc, A.L., Keagle, P., Gellera, C., Ratti, A., Taroni, F., Kwiatkowski, T.J., Jr., McKenna-Yasek, D.M., Sapp, P.C., et al. (2009). Analysis of FUS gene mutation in familial amyotrophic lateral sclerosis within an Italian cohort. Neurology *73*, 1180-1185. 10.1212/WNL.0b013e3181bbff05.
9. Barmada, S.J., Skibinski, G., Korb, E., Rao, E.J., Wu, J.Y., and Finkbeiner, S. (2010). Cytoplasmic mislocalization of TDP-43 is toxic to neurons and enhanced by a mutation associated with familial amyotrophic lateral sclerosis. J Neurosci *30*, 639-649. 10.1523/JNEUROSCI.4988-09.2010.
10. Renton, A.E., Majounie, E., Waite, A., Simon-Sanchez, J., Rollinson, S., Gibbs, J.R., Schymick, J.C., Laaksovirta, H., van Swieten, J.C., Myllykangas, L., et al. (2011). A hexanucleotide repeat expansion in C9ORF72 is the cause of chromosome 9p21-linked ALS-FTD. Neuron *72*, 257-268. 10.1016/j.neuron.2011.09.010.
11. Yun, Y., and Ha, Y. (2020). CRISPR/Cas9-Mediated Gene Correction to Understand ALS. Int J Mol Sci *21*. 10.3390/ijms21113801.
12. Juarez, J.C., Manuia, M., Burnett, M.E., Betancourt, O., Boivin, B., Shaw, D.E., Tonks, N.K., Mazar, A.P., and Donate, F. (2008). Superoxide dismutase 1 (SOD1) is essential for H2O2-mediated oxidation and inactivation of phosphatases in growth factor signaling. Proc Natl Acad Sci U S A *105*, 7147-7152. 10.1073/pnas.0709451105.
13. Nomura, T., Watanabe, S., Kaneko, K., Yamanaka, K., Nukina, N., and Furukawa, Y. (2014). Intranuclear aggregation of mutant FUS/TLS as a molecular pathomechanism of amyotrophic lateral sclerosis. J Biol Chem *289*, 1192-1202. 10.1074/jbc.M113.516492.
14. Mackenzie, I.R.A., and Neumann, M. (2017). Fused in Sarcoma Neuropathology in Neurodegenerative Disease. Cold Spring Harb Perspect Med *7*. 10.1101/cshperspect.a024299.
15. de Boer, E.M.J., Orie, V.K., Williams, T., Baker, M.R., De Oliveira, H.M., Polvikoski, T., Silsby, M., Menon, P., van den Bos, M., Halliday, G.M., et al. (2020). TDP-43 proteinopathies: a new

doi:10.6342/NTU202500138

wave of neurodegenerative diseases. J Neurol Neurosurg Psychiatry *92*, 86-95. 10.1136/jnnp-2020-322983.
16. Babic Leko, M., Zupunski, V., Kirincich, J., Smilovic, D., Hortobagyi, T., Hof, P.R., and Simic, G. (2019). Molecular Mechanisms of Neurodegeneration Related to C9orf72 Hexanucleotide Repeat Expansion. Behav Neurol *2019*, 2909168. 10.1155/2019/2909168.
17. Levine, T.P., Daniels, R.D., Gatta, A.T., Wong, L.H., and Hayes, M.J. (2013). The product of C9orf72, a gene strongly implicated in neurodegeneration, is structurally related to DENN Rab-GEFs. Bioinformatics *29*, 499-503. 10.1093/bioinformatics/bts725.
18. Marat, A.L., Dokainish, H., and McPherson, P.S. (2011). DENN domain proteins: regulators of Rab GTPases. J Biol Chem *286*, 13791-13800. 10.1074/jbc.R110.217067.
19. McAlpine, W., Sun, L., Wang, K.W., Liu, A., Jain, R., San Miguel, M., Wang, J., Zhang, Z., Hayse, B., McAlpine, S.G., et al. (2018). Excessive endosomal TLR signaling causes inflammatory disease in mice with defective SMCR8-WDR41-C9ORF72 complex function. Proc Natl Acad Sci U S A *115*, E11523-E11531. 10.1073/pnas.1814753115.
20. Burberry, A., Suzuki, N., Wang, J.Y., Moccia, R., Mordes, D.A., Stewart, M.H., Suzuki-Uematsu, S., Ghosh, S., Singh, A., Merkle, F.T., et al. (2016). Loss-of-function mutations in the C9ORF72 mouse ortholog cause fatal autoimmune disease. Sci Transl Med *8*, 347ra393. 10.1126/scitranslmed.aaf6038.
21. Sudria-Lopez, E., Koppers, M., de Wit, M., van der Meer, C., Westeneng, H.J., Zundel, C.A., Youssef, S.A., Harkema, L., de Bruin, A., Veldink, J.H., et al. (2016). Full ablation of C9orf72 in mice causes immune system-related pathology and neoplastic events but no motor neuron defects. Acta Neuropathol *132*, 145-147. 10.1007/s00401-016-1581-x.
22. Pang, W., and Hu, F. (2021). Cellular and physiological functions of C9ORF72 and implications for ALS/FTD. J Neurochem *157*, 334-350. 10.1111/jnc.15255.
23. DeJesus-Hernandez, M., Mackenzie, I.R., Boeve, B.F., Boxer, A.L., Baker, M., Rutherford, N.J., Nicholson, A.M., Finch, N.A., Flynn, H., Adamson, J., et al. (2011). Expanded GGGGCC hexanucleotide repeat in noncoding region of C9ORF72 causes chromosome 9p-linked FTD and ALS. Neuron *72*, 245-256. 10.1016/j.neuron.2011.09.011.
24. Waite, A.J., Baumer, D., East, S., Neal, J., Morris, H.R., Ansorge, O., and Blake, D.J. (2014). Reduced C9orf72 protein levels in frontal cortex of amyotrophic lateral sclerosis and frontotemporal degeneration brain with the C9ORF72 hexanucleotide repeat expansion. Neurobiol Aging *35*, 1779 e1775-1779 e1713. 10.1016/j.neurobiolaging.2014.01.016.
25. Belzil, V.V., Bauer, P.O., Prudencio, M., Gendron, T.F., Stetler, C.T., Yan, I.K., Pregent, L., Daughrity, L., Baker, M.C., Rademakers, R., et al. (2013). Reduced C9orf72 gene expression in c9FTD/ALS is caused by histone trimethylation, an epigenetic event detectable in blood. Acta Neuropathol *126*, 895-905. 10.1007/s00401-013-1199-1.
26. Frick, P., Sellier, C., Mackenzie, I.R.A., Cheng, C.Y., Tahraoui-Bories, J., Martinat, C., Pasterkamp, R.J., Prudlo, J., Edbauer, D., Oulad-Abdelghani, M., et al. (2018). Novel antibodies reveal presynaptic localization of C9orf72 protein and reduced protein levels in C9orf72 mutation carriers. Acta Neuropathol Commun *6*, 72. 10.1186/s40478-018-0579-0.
27. Xi, Z., Zinman, L., Moreno, D., Schymick, J., Liang, Y., Sato, C., Zheng, Y., Ghani, M., Dib, S., Keith, J., et al. (2013). Hypermethylation of the CpG island near the G4C2 repeat in ALS with a C9orf72 expansion. Am J Hum Genet *92*, 981-989. 10.1016/j.ajhg.2013.04.017.
28. Shao, Q., Liang, C., Chang, Q., Zhang, W., Yang, M., and Chen, J.F. (2019). C9orf72 deficiency promotes motor deficits of a C9ALS/FTD mouse model in a dose-dependent manner. Acta Neuropathol Commun *7*, 32. 10.1186/s40478-019-0685-7.

doi:10.6342/NTU202500138

29. Ciura, S., Lattante, S., Le Ber, I., Latouche, M., Tostivint, H., Brice, A., and Kabashi, E. (2013). Loss of function of C9orf72 causes motor deficits in a zebrafish model of amyotrophic lateral sclerosis. Ann Neurol *74*, 180-187. 10.1002/ana.23946.
30. Deng, Z., Lim, J., Wang, Q., Purtell, K., Wu, S., Palomo, G.M., Tan, H., Manfredi, G., Zhao, Y., Peng, J., et al. (2020). ALS-FTLD-linked mutations of SQSTM1/p62 disrupt selective autophagy and NFE2L2/NRF2 anti-oxidative stress pathway. Autophagy *16*, 917-931. 10.1080/15548627.2019.1644076.
31. Webster, C.P., Smith, E.F., Grierson, A.J., and De Vos, K.J. (2018). C9orf72 plays a central role in Rab GTPase-dependent regulation of autophagy. Small GTPases *9*, 399-408. 10.1080/21541248.2016.1240495.
32. Beckers, J., and Van Damme, P. (2024). Toxic gain-of-function mechanisms in C9orf72 ALS-FTD neurons drive autophagy and lysosome dysfunction. Autophagy *20*, 2102-2104. 10.1080/15548627.2024.2340415.
33. Haeusler, A.R., Donnelly, C.J., Periz, G., Simko, E.A., Shaw, P.G., Kim, M.S., Maragakis, N.J., Troncoso, J.C., Pandey, A., Sattler, R., et al. (2014). C9orf72 nucleotide repeat structures initiate molecular cascades of disease. Nature *507*, 195-200. 10.1038/nature13124.
34. Kendrick, S., and Hurley, L.H. (2010). The role of G-quadruplex/i-motif secondary structures as cis-acting regulatory elements. Pure Appl Chem *82*, 1609-1621. 10.1351/PAC-CON-09-09-29.
35. Brooks, T.A., Kendrick, S., and Hurley, L. (2010). Making sense of G-quadruplex and i-motif functions in oncogene promoters. FEBS J *277*, 3459-3469. 10.1111/j.1742-4658.2010.07759.x.
36. Ash, P.E., Bieniek, K.F., Gendron, T.F., Caulfield, T., Lin, W.L., Dejesus-Hernandez, M., van Blitterswijk, M.M., Jansen-West, K., Paul, J.W., 3rd, Rademakers, R., et al. (2013). Unconventional translation of C9ORF72 GGGGCC expansion generates insoluble polypeptides specific to c9FTD/ALS. Neuron *77*, 639-646. 10.1016/j.neuron.2013.02.004.
37. Mori, K., Weng, S.M., Arzberger, T., May, S., Rentzsch, K., Kremmer, E., Schmid, B., Kretzschmar, H.A., Cruts, M., Van Broeckhoven, C., et al. (2013). The C9orf72 GGGGCC repeat is translated into aggregating dipeptide-repeat proteins in FTLD/ALS. Science *339*, 1335-1338. 10.1126/science.1232927.
38. Zhang, Y.J., Gendron, T.F., Grima, J.C., Sasaguri, H., Jansen-West, K., Xu, Y.F., Katzman, R.B., Gass, J., Murray, M.E., Shinohara, M., et al. (2016). C9ORF72 poly(GA) aggregates sequester and impair HR23 and nucleocytoplasmic transport proteins. Nat Neurosci *19*, 668-677. 10.1038/nn.4272.
39. Mori, K., Arzberger, T., Grasser, F.A., Gijselinck, I., May, S., Rentzsch, K., Weng, S.M., Schludi, M.H., van der Zee, J., Cruts, M., et al. (2013). Bidirectional transcripts of the expanded C9orf72 hexanucleotide repeat are translated into aggregating dipeptide repeat proteins. Acta Neuropathol *126*, 881-893. 10.1007/s00401-013-1189-3.
40. Mann, D.M., Rollinson, S., Robinson, A., Bennion Callister, J., Thompson, J.C., Snowden, J.S., Gendron, T., Petrucelli, L., Masuda-Suzukake, M., Hasegawa, M., et al. (2013). Dipeptide repeat proteins are present in the p62 positive inclusions in patients with frontotemporal lobar degeneration and motor neurone disease associated with expansions in C9ORF72. Acta Neuropathol Commun *1*, 68. 10.1186/2051-5960-1-68.
41. Wen, X., Tan, W., Westergard, T., Krishnamurthy, K., Markandaiah, S.S., Shi, Y., Lin, S., Shneider, N.A., Monaghan, J., Pandey, U.B., et al. (2014). Antisense proline-arginine RAN

doi:10.6342/NTU202500138

dipeptides linked to C9ORF72-ALS/FTD form toxic nuclear aggregates that initiate in vitro and in vivo neuronal death. Neuron *84*, 1213-1225. 10.1016/j.neuron.2014.12.010.

42. Lee, K.H., Zhang, P., Kim, H.J., Mitrea, D.M., Sarkar, M., Freibaum, B.D., Cika, J., Coughlin, M., Messing, J., Molliex, A., et al. (2016). C9orf72 Dipeptide Repeats Impair the Assembly, Dynamics, and Function of Membrane-Less Organelles. Cell *167*, 774-788 e717. 10.1016/j.cell.2016.10.002.
43. Molliex, A., Temirov, J., Lee, J., Coughlin, M., Kanagaraj, A.P., Kim, H.J., Mittag, T., and Taylor, J.P. (2015). Phase separation by low complexity domains promotes stress granule assembly and drives pathological fibrillization. Cell *163*, 123-133. 10.1016/j.cell.2015.09.015.
44. Shi, K.Y., Mori, E., Nizami, Z.F., Lin, Y., Kato, M., Xiang, S., Wu, L.C., Ding, M., Yu, Y., Gall, J.G., and McKnight, S.L. (2017). Toxic PR(n) poly-dipeptides encoded by the C9orf72 repeat expansion block nuclear import and export. Proc Natl Acad Sci U S A *114*, E1111-E1117. 10.1073/pnas.1620293114.
45. Banani, S.F., Lee, H.O., Hyman, A.A., and Rosen, M.K. (2017). Biomolecular condensates: organizers of cellular biochemistry. Nat Rev Mol Cell Biol *18*, 285-298. 10.1038/nrm.2017.7.
46. Mitrea, D.M., and Kriwacki, R.W. (2016). Phase separation in biology; functional organization of a higher order. Cell Commun Signal *14*, 1. 10.1186/s12964-015-0125-7.
47. Boeynaems, S., Alberti, S., Fawzi, N.L., Mittag, T., Polymenidou, M., Rousseau, F., Schymkowitz, J., Shorter, J., Wolozin, B., Van Den Bosch, L., et al. (2018). Protein Phase Separation: A New Phase in Cell Biology. Trends Cell Biol *28*, 420-435. 10.1016/j.tcb.2018.02.004.
48. Patel, A., Lee, H.O., Jawerth, L., Maharana, S., Jahnel, M., Hein, M.Y., Stoynov, S., Mahamid, J., Saha, S., Franzmann, T.M., et al. (2015). A Liquid-to-Solid Phase Transition of the ALS Protein FUS Accelerated by Disease Mutation. Cell *162*, 1066-1077. 10.1016/j.cell.2015.07.047.
49. Hyman, A.A., Weber, C.A., and Julicher, F. (2014). Liquid-liquid phase separation in biology. Annu Rev Cell Dev Biol *30*, 39-58. 10.1146/annurev-cellbio-100913-013325.
50. Shin, Y., and Brangwynne, C.P. (2017). Liquid phase condensation in cell physiology and disease. Science *357*. 10.1126/science.aaf4382.
51. van Leeuwen, W., and Rabouille, C. (2019). Cellular stress leads to the formation of membraneless stress assemblies in eukaryotic cells. Traffic *20*, 623-638. 10.1111/tra.12669.
52. Banani, S.F., Rice, A.M., Peeples, W.B., Lin, Y., Jain, S., Parker, R., and Rosen, M.K. (2016). Compositional Control of Phase-Separated Cellular Bodies. Cell *166*, 651-663. 10.1016/j.cell.2016.06.010.
53. Martin, E.W., Holehouse, A.S., Peran, I., Farag, M., Incicco, J.J., Bremer, A., Grace, C.R., Soranno, A., Pappu, R.V., and Mittag, T. (2020). Valence and patterning of aromatic residues determine the phase behavior of prion-like domains. Science *367*, 694-699. 10.1126/science.aaw8653.
54. Pak, C.W., Kosno, M., Holehouse, A.S., Padrick, S.B., Mittal, A., Ali, R., Yunus, A.A., Liu, D.R., Pappu, R.V., and Rosen, M.K. (2016). Sequence Determinants of Intracellular Phase Separation by Complex Coacervation of a Disordered Protein. Mol Cell *63*, 72-85. 10.1016/j.molcel.2016.05.042.
55. Bremer, A., Farag, M., Borcherds, W.M., Peran, I., Martin, E.W., Pappu, R.V., and Mittag, T. (2022). Deciphering how naturally occurring sequence features impact the phase behaviours of disordered prion-like domains. Nat Chem *14*, 196-207. 10.1038/s41557-021-00840-w.

doi:10.6342/NTU202500138

56. Lin, Y., Protter, D.S., Rosen, M.K., and Parker, R. (2015). Formation and Maturation of Phase-Separated Liquid Droplets by RNA-Binding Proteins. Mol Cell *60*, 208-219. 10.1016/j.molcel.2015.08.018.
57. Gao, C., Gu, J., Zhang, H., Jiang, K., Tang, L., Liu, R., Zhang, L., Zhang, P., Liu, C., Dai, B., and Song, J. (2022). Hyperosmotic-stress-induced liquid-liquid phase separation of ALS-related proteins in the nucleus. Cell Rep *40*, 111086. 10.1016/j.celrep.2022.111086.
58. Nakagawa, S., Yamazaki, T., and Hirose, T. (2018). Molecular dissection of nuclear paraspeckles: towards understanding the emerging world of the RNP milieu. Open Biol *8*. 10.1098/rsob.180150.
59. Wang, Y., and Chen, L.L. (2020). Organization and function of paraspeckles. Essays Biochem *64*, 875-882. 10.1042/EBC20200010.
60. Latonen, L. (2019). Phase-to-Phase With Nucleoli - Stress Responses, Protein Aggregation and Novel Roles of RNA. Front Cell Neurosci *13*, 151. 10.3389/fncel.2019.00151.
61. Guillen-Chable, F., Bayona, A., Rodriguez-Zapata, L.C., and Castano, E. (2021). Phase Separation of Intrinsically Disordered Nucleolar Proteins Relate to Localization and Function. Int J Mol Sci *22*. 10.3390/ijms222313095.
62. McGurk, L., Gomes, E., Guo, L., Mojsilovic-Petrovic, J., Tran, V., Kalb, R.G., Shorter, J., and Bonini, N.M. (2018). Poly(ADP-Ribose) Prevents Pathological Phase Separation of TDP-43 by Promoting Liquid Demixing and Stress Granule Localization. Mol Cell *71*, 703-717 e709. 10.1016/j.molcel.2018.07.002.
63. Odeh, H.M., and Shorter, J. (2020). Arginine-rich dipeptide-repeat proteins as phase disruptors in C9-ALS/FTD. Emerg Top Life Sci *4*, 293-305. 10.1042/ETLS20190167.
64. Boeynaems, S., Bogaert, E., Kovacs, D., Konijnenberg, A., Timmerman, E., Volkov, A., Guharoy, M., De Decker, M., Jaspers, T., Ryan, V.H., et al. (2017). Phase Separation of C9orf72 Dipeptide Repeats Perturbs Stress Granule Dynamics. Mol Cell *65*, 1044-1055 e1045. 10.1016/j.molcel.2017.02.013.
65. Li, Y.R., King, O.D., Shorter, J., and Gitler, A.D. (2013). Stress granules as crucibles of ALS pathogenesis. J Cell Biol *201*, 361-372. 10.1083/jcb.201302044.
66. White, M.R., Mitrea, D.M., Zhang, P., Stanley, C.B., Cassidy, D.E., Nourse, A., Phillips, A.H., Tolbert, M., Taylor, J.P., and Kriwacki, R.W. (2019). C9orf72 Poly(PR) Dipeptide Repeats Disturb Biomolecular Phase Separation and Disrupt Nucleolar Function. Mol Cell *74*, 713-728 e716. 10.1016/j.molcel.2019.03.019.
67. Kwon, I., Xiang, S., Kato, M., Wu, L., Theodoropoulos, P., Wang, T., Kim, J., Yun, J., Xie, Y., and McKnight, S.L. (2014). Poly-dipeptides encoded by the C9orf72 repeats bind nucleoli, impede RNA biogenesis, and kill cells. Science *345*, 1139-1145. 10.1126/science.1254917.
68. Suzuki, H., Shibagaki, Y., Hattori, S., and Matsuoka, M. (2019). C9-ALS/FTD-linked proline-arginine dipeptide repeat protein associates with paraspeckle components and increases paraspeckle formation. Cell Death Dis *10*, 746. 10.1038/s41419-019-1983-5.
69. Chien, H.M., Lee, C.C., and Huang, J.J. (2021). The Different Faces of the TDP-43 Low-Complexity Domain: The Formation of Liquid Droplets and Amyloid Fibrils. Int J Mol Sci *22*. 10.3390/ijms22158213.
70. Zacco, E., Martin, S.R., Thorogate, R., and Pastore, A. (2018). The RNA-Recognition Motifs of TAR DNA-Binding Protein 43 May Play a Role in the Aberrant Self-Assembly of the Protein. Front Mol Neurosci *11*, 372. 10.3389/fnmol.2018.00372.

doi:10.6342/NTU202500138

71. Francois-Moutal, L., Perez-Miller, S., Scott, D.D., Miranda, V.G., Mollasalehi, N., and Khanna, M. (2019). Structural Insights Into TDP-43 and Effects of Post-translational Modifications. Front Mol Neurosci *12*, 301. 10.3389/fnmol.2019.00301.
72. Acharya, K.K., Govind, C.K., Shore, A.N., Stoler, M.H., and Reddi, P.P. (2006). cis-requirement for the maintenance of round spermatid-specific transcription. Dev Biol *295*, 781-790. 10.1016/j.ydbio.2006.04.443.
73. Buratti, E., and Baralle, F.E. (2001). Characterization and functional implications of the RNA binding properties of nuclear factor TDP-43, a novel splicing regulator of CFTR exon 9. J Biol Chem *276*, 36337-36343. 10.1074/jbc.M104236200.
74. Ayala, Y.M., Zago, P., D'Ambrogio, A., Xu, Y.F., Petrucelli, L., Buratti, E., and Baralle, F.E. (2008). Structural determinants of the cellular localization and shuttling of TDP-43. J Cell Sci *121*, 3778-3785. 10.1242/jcs.038950.
75. Shiina, Y., Arima, K., Tabunoki, H., and Satoh, J. (2010). TDP-43 dimerizes in human cells in culture. Cell Mol Neurobiol *30*, 641-652. 10.1007/s10571-009-9489-9.
76. D'Ambrogio, A., Buratti, E., Stuani, C., Guarnaccia, C., Romano, M., Ayala, Y.M., and Baralle, F.E. (2009). Functional mapping of the interaction between TDP-43 and hnRNP A2 in vivo. Nucleic Acids Res *37*, 4116-4126. 10.1093/nar/gkp342.
77. Wang, H.Y., Wang, I.F., Bose, J., and Shen, C.K. (2004). Structural diversity and functional implications of the eukaryotic TDP gene family. Genomics *83*, 130-139. 10.1016/s0888-7543(03)00214-3.
78. Lagier-Tourenne, C., Polymenidou, M., and Cleveland, D.W. (2010). TDP-43 and FUS/TLS: emerging roles in RNA processing and neurodegeneration. Hum Mol Genet *19*, R46-64. 10.1093/hmg/ddq137.
79. Neumann, M., Sampathu, D.M., Kwong, L.K., Truax, A.C., Micsenyi, M.C., Chou, T.T., Bruce, J., Schuck, T., Grossman, M., Clark, C.M., et al. (2006). Ubiquitinated TDP-43 in frontotemporal lobar degeneration and amyotrophic lateral sclerosis. Science *314*, 130-133. 10.1126/science.1134108.
80. Guenther, E.L., Cao, Q., Trinh, H., Lu, J., Sawaya, M.R., Cascio, D., Boyer, D.R., Rodriguez, J.A., Hughes, M.P., and Eisenberg, D.S. (2018). Atomic structures of TDP-43 LCD segments and insights into reversible or pathogenic aggregation. Nat Struct Mol Biol *25*, 463-471. 10.1038/s41594-018-0064-2.
81. Collins, M., Riascos, D., Kovalik, T., An, J., Krupa, K., Krupa, K., Hood, B.L., Conrads, T.P., Renton, A.E., Traynor, B.J., and Bowser, R. (2012). The RNA-binding motif 45 (RBM45) protein accumulates in inclusion bodies in amyotrophic lateral sclerosis (ALS) and frontotemporal lobar degeneration with TDP-43 inclusions (FTLD-TDP) patients. Acta Neuropathol *124*, 717-732. 10.1007/s00401-012-1045-x.
82. Dammer, E.B., Fallini, C., Gozal, Y.M., Duong, D.M., Rossoll, W., Xu, P., Lah, J.J., Levey, A.I., Peng, J., Bassell, G.J., and Seyfried, N.T. (2012). Coaggregation of RNA-binding proteins in a model of TDP-43 proteinopathy with selective RGG motif methylation and a role for RRM1 ubiquitination. PLoS One *7*, e38658. 10.1371/journal.pone.0038658.
83. Arai, T., Hasegawa, M., Akiyama, H., Ikeda, K., Nonaka, T., Mori, H., Mann, D., Tsuchiya, K., Yoshida, M., Hashizume, Y., and Oda, T. (2006). TDP-43 is a component of ubiquitin-positive tau-negative inclusions in frontotemporal lobar degeneration and amyotrophic lateral sclerosis. Biochem Biophys Res Commun *351*, 602-611. 10.1016/j.bbrc.2006.10.093.
84. Wang, C., Duan, Y., Duan, G., Wang, Q., Zhang, K., Deng, X., Qian, B., Gu, J., Ma, Z., Zhang, S., et al. (2020). Stress Induces Dynamic, Cytotoxicity-Antagonizing TDP-43 Nuclear Bodies

doi:10.6342/NTU202500138

via Paraspeckle LncRNA NEAT1-Mediated Liquid-Liquid Phase Separation. Mol Cell *79*, 443-458 e447. 10.1016/j.molcel.2020.06.019.

85. Yu, H., Lu, S., Gasior, K., Singh, D., Vazquez-Sanchez, S., Tapia, O., Toprani, D., Beccari, M.S., Yates, J.R., 3rd, Da Cruz, S., et al. (2021). HSP70 chaperones RNA-free TDP-43 into anisotropic intranuclear liquid spherical shells. Science *371*. 10.1126/science.abb4309.
86. Wang, A., Conicella, A.E., Schmidt, H.B., Martin, E.W., Rhoads, S.N., Reeb, A.N., Nourse, A., Ramirez Montero, D., Ryan, V.H., Rohatgi, R., et al. (2018). A single N-terminal phosphomimic disrupts TDP-43 polymerization, phase separation, and RNA splicing. EMBO J *37*. 10.15252/embj.201797452.
87. Gopal, P.P., Nirschl, J.J., Klinman, E., and Holzbaur, E.L. (2017). Amyotrophic lateral sclerosis-linked mutations increase the viscosity of liquid-like TDP-43 RNP granules in neurons. Proc Natl Acad Sci U S A *114*, E2466-E2475. 10.1073/pnas.1614462114.
88. Hallegger, M., Chakrabarti, A.M., Lee, F.C.Y., Lee, B.L., Amalietti, A.G., Odeh, H.M., Copley, K.E., Rubien, J.D., Portz, B., Kuret, K., et al. (2021). TDP-43 condensation properties specify its RNA-binding and regulatory repertoire. Cell *184*, 4680-4696 e4622. 10.1016/j.cell.2021.07.018.
89. Streit, L., Kuhn, T., Vomhof, T., Bopp, V., Ludolph, A.C., Weishaupt, J.H., Gebhardt, J.C.M., Michaelis, J., and Danzer, K.M. (2022). Stress induced TDP-43 mobility loss independent of stress granules. Nat Commun *13*, 5480. 10.1038/s41467-022-32939-0.
90. Khalfallah, Y., Kuta, R., Grasmuck, C., Prat, A., Durham, H.D., and Vande Velde, C. (2018). TDP-43 regulation of stress granule dynamics in neurodegenerative disease-relevant cell types. Sci Rep *8*, 7551. 10.1038/s41598-018-25767-0.
91. Babinchak, W.M., Haider, R., Dumm, B.K., Sarkar, P., Surewicz, K., Choi, J.K., and Surewicz, W.K. (2019). The role of liquid-liquid phase separation in aggregation of the TDP-43 low-complexity domain. J Biol Chem *294*, 6306-6317. 10.1074/jbc.RA118.007222.
92. Tamaki, Y., and Urushitani, M. (2022). Molecular Dissection of TDP-43 as a Leading Cause of ALS/FTLD. Int J Mol Sci *23*. 10.3390/ijms232012508.
93. Carey, J.L., and Guo, L. (2022). Liquid-Liquid Phase Separation of TDP-43 and FUS in Physiology and Pathology of Neurodegenerative Diseases. Front Mol Biosci *9*, 826719. 10.3389/fmolb.2022.826719.
94. Li, J., Zhang, M., Ma, W., Yang, B., Lu, H., Zhou, F., and Zhang, L. (2022). Post-translational modifications in liquid-liquid phase separation: a comprehensive review. Mol Biomed *3*, 13. 10.1186/s43556-022-00075-2.
95. Hennig, S., Kong, G., Mannen, T., Sadowska, A., Kobelke, S., Blythe, A., Knott, G.J., Iyer, K.S., Ho, D., Newcombe, E.A., et al. (2015). Prion-like domains in RNA binding proteins are essential for building subnuclear paraspeckles. J Cell Biol *210*, 529-539. 10.1083/jcb.201504117.
96. Yamazaki, T., Souquere, S., Chujo, T., Kobelke, S., Chong, Y.S., Fox, A.H., Bond, C.S., Nakagawa, S., Pierron, G., and Hirose, T. (2018). Functional Domains of NEAT1 Architectural lncRNA Induce Paraspeckle Assembly through Phase Separation. Mol Cell *70*, 1038-1053 e1037. 10.1016/j.molcel.2018.05.019.
97. Nishimoto, Y., Nakagawa, S., Hirose, T., Okano, H.J., Takao, M., Shibata, S., Suyama, S., Kuwako, K., Imai, T., Murayama, S., et al. (2013). The long non-coding RNA nuclear-enriched abundant transcript 1_2 induces paraspeckle formation in the motor neuron during the early phase of amyotrophic lateral sclerosis. Mol Brain *6*, 31. 10.1186/1756-6606-6-31.

doi:10.6342/NTU202500138

98. Tollervey, J.R., Curk, T., Rogelj, B., Briese, M., Cereda, M., Kayikci, M., Konig, J., Hortobagyi, T., Nishimura, A.L., Zupunski, V., et al. (2011). Characterizing the RNA targets and position-dependent splicing regulation by TDP-43. Nat Neurosci *14*, 452-458. 10.1038/nn.2778.
99. Patel, A., Malinovska, L., Saha, S., Wang, J., Alberti, S., Krishnan, Y., and Hyman, A.A. (2017). ATP as a biological hydrotrope. Science *356*, 753-756. 10.1126/science.aaf6846.
100. Mogk, A., Bukau, B., and Kampinga, H.H. (2018). Cellular Handling of Protein Aggregates by Disaggregation Machines. Mol Cell *69*, 214-226. 10.1016/j.molcel.2018.01.004.
101. Udan-Johns, M., Bengoechea, R., Bell, S., Shao, J., Diamond, M.I., True, H.L., Weihl, C.C., and Baloh, R.H. (2014). Prion-like nuclear aggregation of TDP-43 during heat shock is regulated by HSP40/70 chaperones. Hum Mol Genet *23*, 157-170. 10.1093/hmg/ddt408.
102. Gu, J., Wang, C., Hu, R., Li, Y., Zhang, S., Sun, Y., Wang, Q., Li, D., Fang, Y., and Liu, C. (2021). Hsp70 chaperones TDP-43 in dynamic, liquid-like phase and prevents it from amyloid aggregation. Cell Res *31*, 1024-1027. 10.1038/s41422-021-00526-5.
103. He, R.Y., Lai, X.M., Sun, C.S., Kung, T.S., Hong, J.Y., Jheng, Y.S., Liao, W.N., Chen, J.K., Liao, Y.F., Tu, P.H., and Huang, J.J. (2020). Nanoscopic Insights of Amphiphilic Peptide against the Oligomer Assembly Process to Treat Huntington's Disease. Adv Sci (Weinh) *7*, 1901165. 10.1002/advs.201901165.
104. Duan, Y., Du, A., Gu, J., Duan, G., Wang, C., Gui, X., Ma, Z., Qian, B., Deng, X., Zhang, K., et al. (2019). PARylation regulates stress granule dynamics, phase separation, and neurotoxicity of disease-related RNA-binding proteins. Cell Res *29*, 233-247. 10.1038/s41422-019-0141-z.
105. Stanek, D., and Fox, A.H. (2017). Nuclear bodies: news insights into structure and function. Curr Opin Cell Biol *46*, 94-101. 10.1016/j.ceb.2017.05.001.
106. Lam, Y.W., Lamond, A.I., Mann, M., and Andersen, J.S. (2007). Analysis of nucleolar protein dynamics reveals the nuclear degradation of ribosomal proteins. Curr Biol *17*, 749-760. 10.1016/j.cub.2007.03.064.
107. Recasens-Alvarez, C., Alexandre, C., Kirkpatrick, J., Nojima, H., Huels, D.J., Snijders, A.P., and Vincent, J.P. (2021). Ribosomopathy-associated mutations cause proteotoxic stress that is alleviated by TOR inhibition. Nat Cell Biol *23*, 127-135. 10.1038/s41556-020-00626-1.
108. Clerico, E.M., Tilitsky, J.M., Meng, W., and Gierasch, L.M. (2015). How hsp70 molecular machines interact with their substrates to mediate diverse physiological functions. J Mol Biol *427*, 1575-1588. 10.1016/j.jmb.2015.02.004.
109. Gu, J., Liu, Z., Zhang, S., Li, Y., Xia, W., Wang, C., Xiang, H., Liu, Z., Tan, L., Fang, Y., et al. (2020). Hsp40 proteins phase separate to chaperone the assembly and maintenance of membraneless organelles. Proc Natl Acad Sci U S A *117*, 31123-31133. 10.1073/pnas.2002437117.
110. Pedley, A.M., Boylan, J.P., Chan, C.Y., Kennedy, E.L., Kyoung, M., and Benkovic, S.J. (2022). Purine biosynthetic enzymes assemble into liquid-like condensates dependent on the activity of chaperone protein HSP90. J Biol Chem *298*, 101845. 10.1016/j.jbc.2022.101845.
111. Warraich, S.T., Yang, S., Nicholson, G.A., and Blair, I.P. (2010). TDP-43: a DNA and RNA binding protein with roles in neurodegenerative diseases. Int J Biochem Cell Biol *42*, 1606-1609. 10.1016/j.biocel.2010.06.016.
112. Polymenidou, M., Lagier-Tourenne, C., Hutt, K.R., Huelga, S.C., Moran, J., Liang, T.Y., Ling, S.C., Sun, E., Wancewicz, E., Mazur, C., et al. (2011). Long pre-mRNA depletion and RNA missplicing contribute to neuronal vulnerability from loss of TDP-43. Nat Neurosci *14*, 459-468. 10.1038/nn.2779.

doi:10.6342/NTU202500138

113. Duan, L., Zaepfel, B.L., Aksenova, V., Dasso, M., Rothstein, J.D., Kalab, P., and Hayes, L.R. (2022). Nuclear RNA binding regulates TDP-43 nuclear localization and passive nuclear export. Cell Rep *40*, 111106. 10.1016/j.celrep.2022.111106.
114. Rengifo-Gonzalez, J.C., El Hage, K., Clement, M.J., Steiner, E., Joshi, V., Craveur, P., Durand, D., Pastre, D., and Bouhss, A. (2021). The cooperative binding of TDP-43 to GU-rich RNA repeats antagonizes TDP-43 aggregation. Elife *10*. 10.7554/eLife.67605.
115. Modic, M., Grosch, M., Rot, G., Schirge, S., Lepko, T., Yamazaki, T., Lee, F.C.Y., Rusha, E., Shaposhnikov, D., Palo, M., et al. (2019). Cross-Regulation between TDP-43 and Paraspeckles Promotes Pluripotency-Differentiation Transition. Mol Cell *74*, 951-965 e913. 10.1016/j.molcel.2019.03.041.
116. Shan, Q., Ma, F., Wei, J., Li, H., Ma, H., and Sun, P. (2020). Physiological Functions of Heat Shock Proteins. Curr Protein Pept Sci *21*, 751-760. 10.2174/1389203720666191111113726.
117. Freibaum, B.D., Chitta, R.K., High, A.A., and Taylor, J.P. (2010). Global Analysis of TDP-43 Interacting Proteins Reveals Strong Association with RNA Splicing and Translation Machinery. J Proteome Res *9*, 1104-1120. 10.1021/pr901076y.
118. Young, J.C. (2010). Mechanisms of the Hsp70 chaperone system. Biochem Cell Biol *88*, 291-300. 10.1139/o09-175.
119. Powers, M.V., Jones, K., Barillari, C., Westwood, I., van Montfort, R.L., and Workman, P. (2010). Targeting HSP70: the second potentially druggable heat shock protein and molecular chaperone? Cell Cycle *9*, 1542-1550. 10.4161/cc.9.8.11204.
120. Wen, W., Liu, W., Shao, Y., and Chen, L. (2014). VER-155008, a small molecule inhibitor of HSP70 with potent anti-cancer activity on lung cancer cell lines. Exp Biol Med (Maywood) *239*, 638-645. 10.1177/1535370214527899.
121. Gasset-Rosa, F., Lu, S., Yu, H., Chen, C., Melamed, Z., Guo, L., Shorter, J., Da Cruz, S., and Cleveland, D.W. (2019). Cytoplasmic TDP-43 De-mixing Independent of Stress Granules Drives Inhibition of Nuclear Import, Loss of Nuclear TDP-43, and Cell Death. Neuron *102*, 339-357 e337. 10.1016/j.neuron.2019.02.038.
122. Kaminski Schierle, G.S., Bertoncini, C.W., Chan, F.T.S., van der Goot, A.T., Schwedler, S., Skepper, J., Schlachter, S., van Ham, T., Esposito, A., Kumita, J.R., et al. (2011). A FRET sensor for non-invasive imaging of amyloid formation in vivo. Chemphyschem *12*, 673-680. 10.1002/cphc.201000996.
123. Tseng, Y.L., Lu, P.C., Lee, C.C., He, R.Y., Huang, Y.A., Tseng, Y.C., Cheng, T.R., Huang, J.J., and Fang, J.M. (2023). Degradation of neurodegenerative disease-associated TDP-43 aggregates and oligomers via a proteolysis-targeting chimera. J Biomed Sci *30*, 27. 10.1186/s12929-023-00921-7.
124. Guaglianone, G., Torrado, B., Lin, Y.F., Watkins, M.C., Wysocki, V.H., Gratton, E., and Nowick, J.S. (2022). Elucidating the Oligomerization and Cellular Interactions of a Trimer Derived from Abeta through Fluorescence and Mass Spectrometric Studies. ACS Chem Neurosci *13*, 2473-2482. 10.1021/acschemneuro.2c00313.
125. Kayed, R., Head, E., Thompson, J.L., McIntire, T.M., Milton, S.C., Cotman, C.W., and Glabe, C.G. (2003). Common structure of soluble amyloid oligomers implies common mechanism of pathogenesis. Science *300*, 486-489. 10.1126/science.1079469.
126. Fang, Y.S., Tsai, K.J., Chang, Y.J., Kao, P., Woods, R., Kuo, P.H., Wu, C.C., Liao, J.Y., Chou, S.C., Lin, V., et al. (2014). Full-length TDP-43 forms toxic amyloid oligomers that are present in frontotemporal lobar dementia-TDP patients. Nat Commun *5*, 4824. 10.1038/ncomms5824.

doi:10.6342/NTU202500138

127. Chunhui, H., Dilin, X., Ke, Z., Jieyi, S., Sicheng, Y., Dapeng, W., Qinwen, W., and Wei, C. (2018). A11-positive beta-amyloid Oligomer Preparation and Assessment Using Dot Blotting Analysis. J Vis Exp. 10.3791/57592.
128. Mann, J.R., Gleixner, A.M., Mauna, J.C., Gomes, E., DeChellis-Marks, M.R., Needham, P.G., Copley, K.E., Hurtle, B., Portz, B., Pyles, N.J., et al. (2019). RNA Binding Antagonizes Neurotoxic Phase Transitions of TDP-43. Neuron *102*, 321-338 e328. 10.1016/j.neuron.2019.01.048.
129. Perez-Berlanga, M., Wiersma, V.I., Zbinden, A., De Vos, L., Wagner, U., Foglieni, C., Mallona, I., Betz, K.M., Clery, A., Weber, J., et al. (2023). Loss of TDP-43 oligomerization or RNA binding elicits distinct aggregation patterns. EMBO J *42*, e111719. 10.15252/embj.2022111719.
130. Malik, A.M., and Barmada, S.J. (2020). TDP-43 Nuclear Bodies: A NEAT Response to Stress? Mol Cell *79*, 362-364. 10.1016/j.molcel.2020.07.018.
131. Zhang, Y.J., Guo, L., Gonzales, P.K., Gendron, T.F., Wu, Y., Jansen-West, K., O'Raw, A.D., Pickles, S.R., Prudencio, M., Carlomagno, Y., et al. (2019). Heterochromatin anomalies and double-stranded RNA accumulation underlie C9orf72 poly(PR) toxicity. Science *363*. 10.1126/science.aav2606.
132. Hutten, S., Usluer, S., Bourgeois, B., Simonetti, F., Odeh, H.M., Fare, C.M., Czuppa, M., Hruska-Plochan, M., Hofweber, M., Polymenidou, M., et al. (2020). Nuclear Import Receptors Directly Bind to Arginine-Rich Dipeptide Repeat Proteins and Suppress Their Pathological Interactions. Cell Rep *33*, 108538. 10.1016/j.celrep.2020.108538.
133. An, H., de Meritens, C.R., and Shelkovnikova, T.A. (2021). Connecting the "dots": RNP granule network in health and disease. Biochim Biophys Acta Mol Cell Res *1868*, 119058. 10.1016/j.bbamcr.2021.119058.
134. Sun, H., Chen, W., Chen, L., and Zheng, W. (2021). Exploring the molecular basis of UG-rich RNA recognition by the human splicing factor TDP-43 using molecular dynamics simulation and free energy calculation. J Comput Chem *42*, 1670-1680. 10.1002/jcc.26704.
135. McCluggage, F., and Fox, A.H. (2021). Paraspeckle nuclear condensates: Global sensors of cell stress? Bioessays *43*, e2000245. 10.1002/bies.202000245.
136. Lin, Y., Schmidt, B.F., Bruchez, M.P., and McManus, C.J. (2018). Structural analyses of NEAT1 lncRNAs suggest long-range RNA interactions that may contribute to paraspeckle architecture. Nucleic Acids Res *46*, 3742-3752. 10.1093/nar/gky046.
137. Van Treeck, B., and Parker, R. (2018). Emerging Roles for Intermolecular RNA-RNA Interactions in RNP Assemblies. Cell *174*, 791-802. 10.1016/j.cell.2018.07.023.
138. Baborie, A., Griffiths, T.D., Jaros, E., Perry, R., McKeith, I.G., Burn, D.J., Masuda-Suzukake, M., Hasegawa, M., Rollinson, S., Pickering-Brown, S., et al. (2015). Accumulation of dipeptide repeat proteins predates that of TDP-43 in frontotemporal lobar degeneration associated with hexanucleotide repeat expansions in C9ORF72 gene. Neuropathol Appl Neurobiol *41*, 601-612. 10.1111/nan.12178.

doi:10.6342/NTU202500138